A unified rodent atlas reveals the cellular complexity and evolutionary divergence of the dorsal vagal complex

Cecilia Hes[a,b], Abigail J. Tomlinson[c], Lieke Michielsen[d], Hunter J. Murdoch[a,e], Fatemeh Soltani[a,b], Maia Kokoeva[a,e,f], Paul V. Sabatini[a,b,e,f]

[a] Research Institute of the McGill University Health Centre, McGill University Health Centre, 1001 boulevard de Decarie, Montreal, Quebec H4A 3J1, Canada.
[b] Division of Experimental Medicine, Department of Medicine, McGill University, 1001 boulevard de Decarie, Montreal, Quebec H4A 3J1, Canada.
[c] Department of Internal Medicine, University of Michigan, 2600 Plymouth Rd.; NCRC B20E Ann Arbor, MI 48109, USA
[d] Department of Human Genetics, Leiden University Medical Center, P.O. Box 9600, 2300RC Leiden, The Netherlands
[e] Integrated Program in Neuroscience, Department of Medicine, McGill University, Room 302 Irving Ludmer Building, 1033 Pine Ave. W. Montreal, Quebec, H3A 1A1, Canada.
[f] Division of Endocrinology, Department of Medicine, McGill University, 1001 boulevard de Decarie, Montreal, Quebec H4A 3J1, Canada.

Keywords:

DVC, area postrema, nucleus of the solitary tract, cell atlas, PDGFRA

Abstract

The dorsal vagal complex (DVC) is a region in the brainstem comprised of an intricate network of specialized cells responsible for sensing and propagating many appetite-related cues. Understanding the dynamics controlling appetite requires deeply exploring the cell types and transitory states harbored in this brain site. We generated a multi-species DVC cell atlas using single nuclei RNAseq (sn-RNAseq), by curating and harmonizing mouse and rat data, which includes >180,000 cells and 123 cell identities at 5 granularities of cellular resolution. We report unique DVC features such as *Kcnj3* expression in Ca^{+}-permeable astrocytes as well as new cell populations like neurons co-expressing *Th* and *Cck*, and a leptin receptor-expressing neuron population in the rat area postrema which is marked by expression of the progenitor marker, *Pdgfra*. In summary, our findings demonstrate a high degree of complexity within the DVC and provide a valuable tool for the study of this metabolic center.

35 Abbreviations

3v	third ventricle
adj.	adjusted
AMPAr	alpha-amino-3-hydroxy-5-methyl-4-isoxazolepropionic acid receptor
AP	area postrema
APNTS	Area postrema and nucleus of the solitary tract
ARH	arcuate nucleus of the hypothalamus
BAM	binary alignment map
CC	central canal
COE	collier/Olf1/EBF transcription factor
diH_2O	distilled water
DMV	dorsal motor nucleus of the vagus
DVC	dorsal vagal complex
FACS	fluorescence-activated cell sorting
FC	fold-change
GABA	gamma-aminobutyric acid
GDF15	growth differentiation factor 15
GIRK1	G protein-coupled inwardly rectifying potassium channel 1
GLP1R	glucagon-like peptide 1 receptor
GFRAL	GDNF family receptor alpha-like
IR	immunoreactivity
LH	lateral hypothalamus
Lnc	long non-coding
ME	median eminence
Neur	neuronal
NG	*Ng2* glial cell
NS	non-significant
NTS	nucleus of the solitary tract
OL	oligodendrocyte
OPC	oligodendrocyte precursor cell
PC	principal component
PDGFRA	Platelet-derived growth factor receptor A
Res.	resolution
RNA-seq	RNA sequencing
smc	smooth muscle cells

snRNA-seq	single-nuclei RNA sequencing
UMAP	uniform manifold approximation and projection
UMI	unique molecular identifiers
v	version
VGLUT2	vesicular glutamate transporter-2
vr	versus

36

1. Introduction

Regulating appetite in response to changing environmental conditions to maintain energy balance requires the intricate interplay of multiple organs. Within the central nervous system, multiple discrete brain regions and cell types control appetite[1]. More specifically, the dorsal vagal complex (DVC) of the brainstem, comprising the area postrema (AP), nucleus of the solitary tract (NTS) and dorsal motor nucleus of the vagus (DMV), acts as a key nexus point for metabolic signals, evidenced by the dense expression of many relevant hormone receptors[2]. Separately, the DVC also serves as the primary site of gut-based signals via vagal afferents[3-5]. Functionally, the DVC was long considered a site promoting meal termination[6] but growing evidence suggests the DVC also regulates long-term energy balance[7, 8].

Much of the interest in DVC neurons' role in appetite and energy balance stems from their role as therapeutic targets for obesity and anorexia in cancer cachexia[9, 10]. For many years, most pharmacotherapies failed to produce efficacious and long-lasting weight loss in obesity and increase appetite in cancer cachexia[11]. More recently however, the glucagon-like peptide 1 receptor (GLP1R) agonists are eclipsing the weight loss achieved by previous generations of therapeutics[12]. While expressed across the central nervous system, GLP1R expression is particularly enriched in DVC neurons[13] and it is the DVC that mediates many of the effects of GLP1R agonists[14]. Separately, an emerging strategy for treating cancer cachexia is inhibiting growth differentiation factor 15 (GDF15) signaling in the DVC by blocking the action of GDNF Family Receptor Alpha Like (GFRAL)[15], the receptor for GDF15[16]. Given the clinical significance of the DVC for this spectrum of conditions, understanding the molecular heterogeneity and function of this region is essential to therapeutically altering appetite while avoiding side effects.

Traditionally, identification and ensuing study of DVC cell types was limited to known neurotransmitter and receptor-expressing cell types. For instance, the cholecystokinin and monoamine-expressing cells, demarcated by tyrosine hydroxylase (*Th*) expression, were previously shown to be non-overlapping cell populations with unique roles in appetite suppression[17]. More recently, the advent of single-cell mRNA sequencing approaches made unbiased molecular censuses of heterogenous populations possible. Such studies focusing on the mouse have revealed the complexity of the mouse DVC, comprised of dozens of transcriptionally distinct cell types[2, 18, 19]. Moving forward, unifying information from multiple single-nuclei RNA sequencing (snRNA-seq) datasets of the DVC into a reference atlas is needed to more fully understand the cells within the DVC and generate a common and scalable classification for cell identities. Such a reference atlas is also needed to contrast

the cell types found within the mouse to other research models, including the rat, which are prominent models for DVC biology[2, 20].

To address this, we generated a comprehensive snRNA-seq based atlas of the mouse and rat DVC. This atlas features mouse and rat labelled cells with increasing granularity and an accompanying computational toolbox including the mouse and rodent atlas label transfer environment using treeArches. The mouse DVC atlas reveals a higher degree of cellular complexity than previously appreciated. The cellular census of the rat DVC exhibits many similarities to the mouse but also rat-specific cells including a novel population of leptin receptor and *Pdgfra*-expressing neurons localized to the AP. Using this unified atlas, we also uncover the cell types that transcriptionally respond to meal consumption which may hold the potential of suppressing appetite without gastrointestinal side effects.

2. Materials and methods

2.1. Experimental design

To generate a snRNA-Seq based atlas of the mouse dorsal vagal complex (DVC), we isolated the DVC from 30 adult C57BL/6J mice and subjected them to 10x Genomics-based single-nuclei RNA barcoding and sequencing. Mice were either fasted overnight (n=5), fasted overnight and then refed 2 hours prior to euthanasia (n=10), fed ad libitum (n=5), injected with LiCl (n=5) or injected with vehicle (n=5). Conserved cell clusters across these groups were then identified.

2.2. Animals

All animals were bred in the Unit for Laboratory Animal Medicine at the University of Michigan and the Research Institute of the McGill University Health Centre. Procedures performed were approved by the University of Michigan Committee on the Use and Care of Animals, in accordance with Association for the Assessment and Approval of Laboratory Animal Care and National Institutes of Health guidelines. Alternatively, procedures were approved by the animal care committee of McGill University.

2.2.1. Mouse tissue for sn-RNA sequencing assay

Wild-type C57BL/6J mice (Jackson laboratories) were given ad libitum access to food (Purina Lab Diet 5001) and water in temperature-controlled (22°C) rooms on a 12-hour light-dark cycle with daily health checks. Mice were euthanized by isoflurane anesthesia and decapitated, then the brain was removed from the skull and aligned in a brain matrix. The cerebellar cortex was removed and the DVC was micro-dissected using AP-centric targeting and flash frozen in liquid nitrogen (Fig.S1). To limit any circadian-driven gene expression

111 changes, all animals were euthanized 4 hours following the onset of the light phase. Frozen
112 tissue was stored at -80°C until use.
113
114 For assessment of feeding-related gene expression, mice were either ad libitum fed or food
115 was removed at the onset of the dark cycle and the animals were fasted overnight. Animals
116 were then euthanized the next morning under ad libitum fed or fasting conditions. A subset
117 of fasted animals (n=5) were provided food and allowed to refeed for 2 hours prior to
118 euthanasia.
119
120 2.2.2. Mouse and rat tissue collection for *in-situ* hybridization and
121 immunofluorescent assays
122 Mice were provided with ad libitum access to food (Purina Lab Diet 5001) and water in
123 temperature-controlled (22°C) rooms on a 12 h light-dark cycle with daily health status
124 checks. C57BL/6J mice (Jackson laboratories) or Sprague Dawley (Jackson laboratoties)
125 were euthanized by isoflurane anesthesia followed by CO_2 asphyxiation. Animals were then
126 trans-cardially perfused with phosphate buffered saline for 3 minutes followed by 5 minutes
127 perfusion with 10% formalin. Brain tissue was then collected and postfixed for 24 hours in
128 10% formalin before transfer into 30% sucrose for a minimum of 24 hours. Brains were then
129 sectioned as 30 μm thick, free-floating sections.
130
131 2.2.3. Rat tissue collection for snRNA sequencing assays
132 Wild-type Sprague Dawley rats (Charles River) were provided with given access to food
133 (Purina Lab Diet 5001) and water in temperature-controlled (22°C) rooms on a 12-hour light-
134 dark cycle with daily health checks. Rats were euthanized by intraperitoneal injections of
135 pentobarbital and decapitated, then the brain was removed from the skull and aligned in a
136 brain matrix. The cerebellar cortex was removed and the DVC was dissected out in an AP-
137 centric manner then flash frozen in liquid nitrogen. Frozen tissue was stored at -80°C until
138 use.
139
140 2.3 Isolation of nuclei from DVC tissue
141 Frozen tissue was pooled (5 pooled DVC from mice and 2 DVCs from rats) and homogenized
142 in Lysis Buffer (EZ Prep Nuclei Kit, Sigma-Aldrich) with Protector RNAase Inhibitor (Sigma-
143 Aldrich) and filtered through a 30mm MACS strainer (Miltenyi). Filtered samples were
144 centrifuged at 500 rcf for 5 minutes at 4°C, and pelleted nuclei were resuspended in fresh-
145 made wash buffer (10 mM Tris Buffer, pH 8.0, 5 mM KCl, 12.5 mM MgCl2, 1% BSA with
146 RNAse inhibitor) before undergoing a second filtration and centrifugation. The pelleted nuclei
147 were resuspended in wash buffer with propidium iodide (Sigma-Aldrich) and underwent

148 fluorescence-activated cell sorting (FACS) on a MoFlo Astrios Cell Sorter to remove debris.
149 PI+ nuclei were collected and centrifuged at 100 rcf for 5 minutes at 4°C and resuspended
150 in wash buffer to obtain a concentration of 750-1,200 nuclei/μL in preparation for sequencing.
151
152 ### 2.4. Single-nuclei RNA-sequencing
153 Library preparation was handled by the Advanced Genomics Core at the University of
154 Michigan. RT mix was added to target approximately 10,000 nuclei recovered per sample
155 and loaded onto the 10× Chromium Controller chip. The Chromium Single Cell 3′ Library and
156 Gel Bead Kit v3, Chromium Chip B Single Cell kit, and Chromium i7 Multiplex Kit were used
157 for subsequent RT, cDNA amplification, and library preparation, as instructed by the
158 manufacturer. Libraries were sequenced on an Illumina NovaSeq 6000 (pair ended with read
159 lengths of 150 nt).
160
161 ### 2.5. Processing of the snRNA-sequencing files
162 From the snRNA-seq, we obtained four FASTQ files (two per sequencing lane, containing
163 forward and reverse sequences respectively) per mouse treatment and two files with the
164 forward and reverse sequences for the rat samples. We pre-processed the murine FASTQ
165 files using either CellRanger 5.0.1 with inclusion of introns or CellRanger 7.0.1 with default
166 parameters (which include intronic sequences) to align sequencing reads to the murine
167 genome[21]. We aligned to the *Mus musculus* refdata-gex-mm10-2020-A reference genome.
168 For the rat files, we used CellRanger 3.0.1 with no introns inclusion and aligned using the
169 *Rattus norvegicus* genome assembly Rnor_6.0[21]. We obtained 110,167 and 13,360 cells
170 from the murine and rat experiments, respectively. In addition to these two datasets, we also
171 used the following steps to process the murine Dowsett dataset[18] publicly available as a
172 raw gene expression matrix set of files. We processed the gene expression matrices in R[22]
173 with Seurat v5 and SeuratObject v5 to remove low quality cells[23]. For processing and
174 analysis, R v4.3.1[22] was used. We filtered cells with ≥500 number of genes mapped and
175 >1.22 RNA unique molecular identifiers (UMIs) counts/genes mapped ratio (based on the
176 first 2 percentiles per sample) (**Table S1**). Subsequently, we merged the data per treatment,
177 calculated the median RNA content of clusters at resolution 1.0 and those below the first
178 quartile of the median distribution were removed (**Table S2**). Additionally, we used
179 DoubletFinder v2.0.3 based on the expected doublets rates by 10X Genomics after adjusting
180 for homotypic doublets modeled as the sum of squared annotation frequencies[24] (**Table**
181 **S3**). On each iteration we processed the data with libraries scaled to 10,000 UMIs per cell
182 and log-normalized. We identified the most variable genes computing a bin Z-score for
183 dispersion based on 20 bins average expression. We regressed UMI counts and used
184 principal component (PC) analysis for dimensionality reduction on to the top 2,000 most

185 variable genes. We used the first 30 PCs for *k*-nearest neighbors clustering and for uniform
186 manifold approximation and projection (UMAP) projections using Seurat v5[23] default
187 parameters. Murine samples integration in a single matrix was done with Harmony[25], after
188 which clustering and UMAP projections were performed using the harmony embeddings
189 instead of PCs.
190
191 **2.6. Mapping of our murine data to existing brain databases**
192 We mapped the resulting murine integrated high quality singlets to the celldex v1.12.0 built-
193 in mouse RNA sequencing reference and other four mouse databases[26-29] (**Table S4**)
194 using SingleR v2.4.1[30] and scRNA-seq v2.16.0[31] packages in R[22]. Since each
195 database has its own cell type nomenclature, in our murine dataset we established a 'likely-
196 cell type' to be unanimous among all databases, for example if all databases labeled a cell
197 as 'neuron'. We initially labeled the cells with conflicting or unassigned label by one or more
198 databases as 'unknown'. In order to confirm the cell type of all the cells labeled and to identify
199 the unknown cell identities, we mapped 473 markers from the literature. For this, the average
200 expression per marker gene was obtained on scaled data for each cluster at resolution 1.0
201 (i.e. 48 clusters) (**Table S5**). We also manually visualized UMAP projections from all these
202 markers in our dataset. Some clusters (e.g. cluster 27) showed in the previous step to contain
203 cells belonging to different cell types, so we subset and reprocessed these clusters using
204 the Harmony embeddings to assign their cell identity based on marker expression at the
205 lowest resolution level that allowed to separate them.
206
207 **2.7. Assigning high resolution clustering-based cell identity in the murine dataset**
208 In the murine dataset, for all non-neuronal clusters at resolution 1.0 gene expression markers
209 were obtained using the FindConservedMarkers function from Seurat v5[23] package in
210 R[22]. The function was run using the MAST algorithm[32] on scaled data with a log fold-
211 change (FC) threshold of 0.25. Only upregulated marker genes detected on 40% of all cells
212 in that cluster, were retained. Since the FindConservedMarkers gives a log2FC output per
213 sample, we calculated the average log2FC across samples and the proportion of samples
214 for which a gene had an adjusted p-value ≤ 0.05. A marker gene was considered as such if it
215 had an average log2FC>1 across samples and was significant (i.e. had an adjusted p-value
216 ≤ 0.05) in more than 80% of the samples. Furthermore, neurons were subset, reprocessed
217 and subjected to new clustering through Seurat v5[23]. We obtained the gene markers per
218 cluster at resolution 1.0 as described. We named the clusters based on the known functions
219 of the upregulated/downregulated genes (e.g. myelinating oligodendrocytes), peculiarities of
220 the cell groups (e.g. Ca^{+}-permeable astrocytes) or their upregulated gene expression
221 markers if the previous methods were unsuitable (e.g. Ano2 neurons) (**Table S6**). All

visualizations, unless otherwise stated, were done using ggplot2 v3.5.0 and ComplexHeatmap v2.18.0 packages in R[22].

2.8. Oligodendrocytes trajectory inference

We subset the oligodendrocytes (i.e. pre-myelinating, myelinating intermediate and myelinating) in our murine dataset and placed each cell on an inferred cellular trajectory using their transcriptomic data in R[22]. We used the SCORPIUS v1.0.9 package[33] with default parameters to perform dimensionality reduction by PCA on log-normalized counts and to obtain the trajectory image, with a random seed of 1,000. We additionally performed the analysis on the Harmony embeddings from the original data integration.

2.9. Gene expression files format interconversions

To convert Seurat ('RDS') DVC datasets to 'h5ad' format and vice versa, we used reticulate v1.35.0[34] and anndata 0.7.5.6[35] packages in R[22] with import of scipy, scanpy, numpy and anndata modules from Python v3.9[36]. To convert .txt, .csv and .tsv datasets (i.e. the Ludwig dataset[2], the spinal cord dataset[37] and the cortex/hippocampus database[38]), we converted those to 'h5ad' format in Python v3.9[36].

2.10. Murine DVC hierarchy construction

We converted our murine labeled count matrix to h5ad. We used treeArches[39] in Python v3.9[36] to create a manual tree using the three layers of cellular granularity in our database. We reprocessed the samples using the treeArches pipeline[39] to normalize the count data (counts normalized per cell and then log-normalized), identify the top 2,500 most variable genes and integrate the samples using scVI[40]. This reference latent space obtained after integration was used to generate the UMAP embeddings. We trained our manual tree based on the cell identity layer-3 labels using default parameters.

We subset the Ludwig dataset[2] to match the initial 2,500 most variable genes from our datasets and performed surgery to incorporate labels from the Ludwig dataset[2]. The two layers of granularity established by Ludwig[2] were combined in the variable "identity_layer3" to contain the highest granularity of cell identity for neurons and non-neuronal cell types. Next, we normalized the count data as specified for our murine dataset, and mapped the Ludwig dataset on the reference latent space using scArches. We then used the learn_tree function with default parameters for hierarchical progressive learning from scHPL v1.0.5[41] which yielded a hierarchy of harmonized cell labels from both datasets. We printed all trees using matplotlib v3.8.2[42] and scHPL v1.0.5[41]. All steps performed and scripts used in

258 this phase are available in the GitHub repository:
259 https://github.com/LabSabatini/DVC_cell_atlas.
260
261 2.10.1. Corroboration of the validity of our murine cell hierarchy using treeArches
262 prediction modality
263 Using treeArches[39] and its dependencies in Python v3.9[36] we compared the original cell
264 labels in our and Ludwig datasets with the resulting prediction of the label for each cell using
265 our learned hierarchy. We used the predict_labels function from scHPL v1.0.5[41] with default
266 parameters, and the latent representation obtained when we constructed our murine
267 hierarchy. We compared the original and the predicted labels through a heatmap
268 visualization. Next, we predicted the labels of new data, a murine dataset by Dowsett which
269 comprises the NTS, a part of the DVC[18]. We processed the Dowsett data similarly to the
270 Ludwig dataset and obtained the query latent representation. We then used the
271 predict_labels function from scHPL v1.0.5[41] with default parameters to transfer the labels
272 in our hierarchy to the Dowsett dataset based on gene expression similarity among the 2,500
273 initial most variable genes. We then compared the resulting labels from this prediction to the
274 manual mapping of our cell identities based on maker expression (Table S7) using UMAP
275 embeddings in R[22].
276
277 2.11. Labeling of our rat DVC dataset
278 We processed our rat dataset as previously described to obtain high-quality singlets. Based
279 on the three layers of cell identity that we created to label the murine data from our
280 experiments, we calculated the average expression of the top 5 marker genes for each of the
281 layer-3 identities (except duplicated genes and mouse-specific genes) on every rat cluster
282 to identify those that were equivalent and could be labeled as the murine data (Tables S6
283 and S8). Since this dataset is smaller than the mouse data, we decided to use clusters at
284 resolution of 2.0 to capture more heterogeneity and delineate better the non-neuronal cell
285 populations. Clusters 27 and 29 were further subset and reclustered since we found them to
286 contain a mix of endothelial cells, mural cells, tanycytes and fibroblasts based on marker
287 expression. Microglia and mixed neurons were sub-clustered as well. The lowest resolution
288 level that allowed to separate populations was used to label the cells. Neurons were also
289 subset and we mapped the murine neuronal classes markers to resolution 2.0 markers which
290 were manually curated to delineate better the different populations within them. For all cell
291 identities, and because we only applied one treatment to the rats (i.e. fed ad libitum), we
292 used the FindMarkers function from Seurat v5[23] package in R[22] to obtain gene
293 expression markers of each rat cell population. The function was run using the MAST
294 algorithm[32] with same parameters used for the murine data (Table S9).

295
296 ### 2.12. Construction of the rodent DVC hierarchy
297 We then integrated our rat labeled dataset to the murine samples in Python v3.9[36] using
298 the initial top 2,500 most variable genes initially defined in our mouse data. Incorporation of
299 rat labels was done as previously described for the Ludwig dataset using the learn_tree
300 function for hierarchical progressive learning from scHPL v1.0.5[41]. The cell populations that
301 were not rejected but placed at the bottom of the tree were moved manually to their belonging
302 parent branches. For example, the 'smooth_muscle_rat' label was moved to be a children
303 node of the mural cells node. If the parent branch did not exist, we created it. For example,
304 the 'immunity_related_rat' label belonged to a new rat neuronal class, therefore, we
305 incorporated this parent node within the neurons node and then we moved the
306 'immunity_related_rat' label to be a children node. After manual curation, we re-trained the
307 tree. We printed all trees using matplotlib v3.8.2[42] and scHPL v1.0.5[41]. All steps
308 performed and scripts used in this phase are available at the GitHub repository
309 https://github.com/LabSabatini/DVC_cell_atlas for reproducibility.
310
311 ### 2.13. Mapping gene expression in other brain-site snRNA-seq datasets
312 We downloaded labeled datasets from six brain regions different from the DVC: the
313 HypoMap, spinal cord, cortex, hippocampus, pons and forebrain databases[37, 38, 43, 44].
314 For the HypoMap data, we subset the database by randomly selecting cells belonging to 32
315 included hypothalamic samples. We processed the datasets in Seurat v5[23] as previously
316 described and obtained Harmony[25] embeddings to obtain UMAP projections. The labels
317 used in the visualization are the original curated labels provided on each dataset. Neurons
318 were further subset from the processed datasets and reprocessed as previously described.
319 The other datasets were processed in the same manner after subsetting astrocytes. The pons
320 and forebrain data was downloaded using in scRNAseq v2.16.0 packages in R through
321 SingleR v2.4.1[30].
322
323 ### 2.14. Differential gene expression analysis in murine treatments
324 We subset the murine dataset neurons and glial cells at layer 2 granularity of identity and
325 obtained differential gene expression for pair-wise comparison of treatments (i.e. refed
326 versus ad libitum fed, refed versus fasted and LiCl versus vehicle injected mice). We used
327 the FindMarkers function from Seurat v5[23] package in R[22] using the MAST algorithm[32]
328 on log-normalized counts with a minimal log fold-change threshold of 0.1 and default
329 parameters. The number of cells per treatment can be found in **Table S10**.
330
331 ### 2.15. Immunofluorescent staining

332 Free-floating brain sections from mouse and rat were washed with PBS, three times for five
333 minutes. The sections were then blocked for one hour in PBS containing 0.1% Triton X-100
334 and 3% normal donkey serum (Fisher Scientific). The sections were incubated overnight at
335 room temperature with Goat anti-PDGFRA (Invitrogen, CAT#, 1:200), HuC/HuD (Invitrogen,
336 A-21271, 1:30). The following day, sections were washed and incubated for two hours with
337 Alexflour488 and Cy3 conjugated secondary antibody (Jackson immunoresearch, 1:500).
338 Tissues were then washed three times in PBS before being mounted onto glass slides,
339 covered in mounting media (Fluoromount-G, Southern Biotechnology) and coverslipped.
340 Imaging was performed using an Olympus BX61 microscope and a Zeiss LSM780-NLO laser
341 scanning confocal microscope equipped with IR-OPO lasers at the Molecular Imaging
342 Platform, Research Institute of the McGill University Health Centre (RI-MUHC), Montreal, CA.
343

344 2.16. *In-situ* hybridization and imaging

345 Brain sections containing the DVC from four wild-type C57BL/6J mice obtained as described
346 above, were fixed on glass slides and stored at -20°C for no more than 36 hours. We followed
347 the manufacturer's ACD 323100 user manual for the RNAscope® Multiplex Fluorescent
348 Reagent Kit v2 Assay for fixed frozen tissue samples. Briefly, we rinsed the slides with 1X
349 PBS and incubated them at room temperature for 10 minutes after adding ~1-2 drops of H_2O_2
350 per section. We removed the H_2O_2 from slides and rinsed them twice with distilled water
351 (diH_2O). Next, we submerged the slides in 200 mL of hot diH_2O for 10 seconds followed by
352 200mL of RNAscope® 1X Target Retrieval Reagent for 5 minutes, using a steamer with lid.
353 After briefly transferring the slides to room temperature diH_2O, we submerged them in 100%
354 ethanol for 3 minutes and allowed them to air dry. We applied approximately 1-2 drops of
355 RNAscope® Protease III to each section and incubated them at 40°C for 30 minutes in a
356 HybEZ™ oven with diH_2O wet paper in the tray. After rinsing the slides with diH_2O, we
357 hybridized the probes at 40°C for 2 hours.
358

359 From this point on, we performed all steps by incubating the slides at 40°C in the HybEZ™
360 oven with humid tray followed by rinse using RNAscope® 1X Wash Buffer. We applied
361 approximately 1-2 drops of RNAscope® reagents AMP1, AMP2, AMP3 and then intercalated
362 HRP channel (15 minutes), fluorophore (30 minutes) and HRP blocker (15 minutes) for each
363 channel present in the probe mix. The mix of probes used for the *Th*/*Cck* co-expression assay
364 was RNAscope® Mm-Th-C2 (317621-C2) and Mm-Cck-C3 (402271-C3) diluted in probe
365 diluent as specified in the user manual. For *Hcrt* we used RNAscope® Mm-Hcrt-C2 (490461-
366 C2) and for *Agrp*, Mm-Agrp (400711), in a dilution as specified in the user manual. The used
367 fluorophores were Cy3 for *Cck* and *Hcrt* (1:1,500), and Cy5 for *Th* and *Agrp* (1:1,000) diluted

368 in RNAscope® TSA buffer. DAPI dye (1:1,000) was applied at the end of the assay, and the
369 samples were stored for ~48 hours at -4°C, protected from light, before imaging. We imaged
370 the sections using a Zeiss LSM780-NLO laser scanning confocal microscope with IR-OPO
371 lasers at the Molecular Imaging Platform at the RI-MUHC, Montreal, CA.
372
373 ## 3. Results
374 ### 3.1. The murine dorsal vagal complex cell classes
375 To generate a *de novo* snRNA-seq atlas of the mouse DVC, we isolated the DVC from 30
376 adult C57BL/6J mice and subjected them to 10X Genomics-based snRNA barcoding and
377 sequencing (**Fig.1A**). From the CellRanger pre-processing pipeline[21] we obtained 110,167
378 cells of which 99,740 were retained after processing. Cell identities were initially mapped to
379 5 databases from different brain regions and then curated manually using 473 cell identity
380 markers (**Tables S4-S5**). We distinguished clusters of neurons and glial, vascular and
381 connective tissue cells, a first layer of cell identity (**Fig.1B**; **Table S9**). We further describe a
382 second layer of cellular resolution, which are subgroups of the first layer that contain the cell
383 classes (**Fig.1C**; **Table S7**).
384
385 Among the ten neuronal cell classes identified at layer 2 resolution, we found two major
386 groups which we called 'magnaclass1' and 'magnaclass2' (**Fig.S2**). Magnaclass1 neurons
387 predominately express genes required for inhibitory neurotransmission (e.g. *Gad1*, *Gad2*)
388 and share transcriptomic markers with the Sall3-class of neurons, whereas magnaclass2
389 neurons express mostly excitatory transcripts (e.g. the glutamate transporter VGLUT2) also
390 found in the Lhx2-class and monoamine-class (**Fig.1D-E**; **Fig.S2**). However, as described in
391 other brain areas[45, 46], evidence of co-transmission/co-release of multiple primary
392 neurotransmitters was found in at least 55% of neurons regardless of their cell class (**Fig.1D-**
393 **E**; **Table S11**). We also identified 8 transcriptionally distinct neural classes in addition to the
394 magnaclasses. Among these 8 classes we found two neural classes expressing traditionally
395 non-neuronal genes; the Golli and pH-related classes. The Golli-class neurons are a relatively
396 small cluster, comprising ~1% of all neurons. Interestingly, Golli-class neurons express
397 multiple myelin-associated genes such as *Mag* and *Mog*[47-49] normally expressed by
398 oligodendrocytes (**Fig.1D**; **Table S6**). Additionally, we identified a class of neurons with genes
399 normally upregulated in astrocytes (e.g. *Slc6a11*) and related to clearance and uptake of
400 glutamate, gamma-aminobutyric acid (GABA), Ca^{+} and bicarbonate [50, 51], which we
401 named 'pH-related class' (**Table S6**). Similar to Golli-class neurons, pH-related neurons were
402 a relatively rare cluster (<1% of all neurons). While the corelautus-class neurons express very
403 few genes at higher levels, among them are *Cdk8*, *Lars2*, *Gabra6* and *Fat2*. Expression of
404 *Cdk8* is largely absent from the DVC but is enriched within the DVC-adjacent hypoglossal

405 nucleus (Fig.S3) suggesting these cells are hypoglossal neurons. We also identified the Lhx2-
406 Class which was enriched for the Parvalbumin (*Pvalb*) gene whose expression is largely
407 excluded from the DVC. As *Pvalb* is highly expressed in the neighbouring cuneate nucleus
408 (Fig.S3), we posit this class may belong to this anatomically adjacent area which was
409 captured in our dissection. When interrogating snRNA-seq data from the hypothalamus[43]
410 (Fig.S4), another brain site important for energy balance, we could not find clusters sharing
411 all markers with our neuronal classes, indicating DVC-specific neuronal programs (Fig.S4C).
412

413 ### 3.2. The murine DVC cells at their highest resolution

414 To better define the heterogeneity of the mouse DVC, we further assigned a clustering-based
415 third layer of cellular resolution resulting in fifty cell identities, of which 15 are non-neuronal
416 (Fig.2A). At this resolution we differentiated between two major groups of astrocytes.
417 Differential expression in synapse-related factors revealed a group of highly excitable
418 astrocytes with high expression of the inwardly rectifying GIRK1 (*Kcnj3*) channel[52] and lack
419 of expression of the AMPAr subunit GluA2 (*Gria2*), additionally rendering them K^+/Na^+/Ca^+-
420 permeable[53, 54] (Fig.2B). We speculate these astrocytes are specific to the DVC as we
421 could not find *Kcnj3*+; *Gria2*- astrocytes in the hypothalamus, forebrain, cortex or
422 hippocampus[38, 43, 44] (Fig.S4D; Fig.S5). Furthermore, although some regions close to the
423 DVC such as pons and the spinal cord show some co-expression of *Kcnj3* and *Gfrap*, the
424 patterns are not to the same extent as observed in the DVC [44] (Fig.S5F-G). In addition, we
425 distinguished a spectrum of DVC mature oligodendrocytes, including a group resembling the
426 intermediate oligodendrocytes described in the other brain sites that decrease in number
427 with age[37, 55] (Fig.2C). This gradient of expression of markers including *Fyn*, *Opalin* and
428 *Anln* in oligodendrocytes (Fig.2C), do not respond to a developmental trajectory (Fig.S6).
429 Although 'myelinating-intermediate' and 'myelinating' oligodendrocytes include cells with
430 overlapping gene expression programs, there is no evidence that each oligodendrocyte will
431 follow a single trajectory (Fig.S6). Furthermore, to properly separate some cell identities, we
432 performed sub-clustering in three DVC clusters (i.e. clusters 23, 26 and 27) (Fig.S7A). This
433 permitted us to label pre-myelinating oligodendrocytes, endothelial and mural cells, and
434 distinguish two fibroblast sub-types (Fig.S7). One of these subtypes expresses high *Stk39*
435 previously described in fibroblast stress-response[56] and so was termed 's-fibroblasts' for
436 stress-associated fibroblasts (Fig.S7B), which we failed to detect in the hypothalamus
437 (Fig.S4E). Additionally, we excluded the possibility of monocytes in our microglial data
438 (Fig.S8A), which had no evidence of microglial activation as we mapped minimal levels of
439 the activation genes *Cxcl10*, *Cd5*, *Cxcl9* and *Zbp1*[57], therefore we posit that our DVC
440 microglial cells are in a basal state (Fig.S8B). To further evaluate possible activation states in
441 microglia, we performed sub-clustering and evaluated their marker genes (Fig.S8C). We

442 have identified a group of microglia expressing oligodendrocyte markers and resembling a
443 subpopulation of hippocampal microglia in an Alzheimer's disease model which is disease-
444 protective and synaptic-function-supporting[58], and a cortical/subcortical phagocytic
445 subpopulation in a multiple sclerosis model[59]. A second group expresses *Ndrg2* and
446 receptors for GABA and glutamate which have been related to microglia that may induce
447 neuronal damage[60, 61] (Fig.S8D).
448
449 We also obtained the DVC gene expression markers of the main cell types in the central
450 nervous system and neurons (Fig.2D). To more thoroughly classify DVC neural types, we
451 subset and re-clustered the 10 neural classes from layer 2 which resulted in 35 neuronal
452 identities as a third layer of granularity (Fig.3A; Table S6). These identities include
453 'preganglionic' or *Chat*-expressing neurons and a large number of neurons with unspecific
454 markers which we called 'mixed neurons' (Table S6). Of the mixed neuron classes, two are
455 largely excitatory (Mixed neurons 3 and 4) and two largely inhibitory, however, cells in the
456 four mixed neuron classes share similar transcriptional profiles with many other neural
457 classes. When we performed sub-clustering on mixed neurons, we could distinguish a total
458 of 10 subtypes from the original 4 mixed neuronal identities (Fig.S9); however, transcriptional
459 differences between these were subtle. Interestingly, a mixed neurons-like group of cells was
460 previously described in the murine hypothalamus[26], suggesting multiple brain sites may
461 contain neurons which lack highly differentiable transcriptional programs from snRNA-
462 sequencing data.
463
464 Additionally, we split the monoamine-class into four layer-3 cell identities (i.e. M0, M1, M2
465 and M3) with specific cell markers (Fig.3B; Table S6). M0 and M1 neurons express genes for
466 enzymes synthesizing norepinephrine and serotonin, but M0 expresses minimal levels of the
467 transporter VMAT2 (*Slc18a2*) (Fig.3C; Table S6). Due to the low proportion of cells expressing
468 *Th* and *Tph2* in M2 and M3 neurons, we consider them monoamine-modulators as they seem
469 to synthesize trace amines (Fig.3C; Table S6). Of note, the receptor for GDF15, GFRAL, is
470 expressed heavily by a subset of M0 neurons, some of which co-express the calcium sensing
471 receptor (*Casr*) gene (Fig.3C).
472
473 We named 'GLP1' a neuronal cluster with high expression of the pre-proglucagon gene (*Gcg*)
474 (Fig.3D; Table S6), which also expresses high levels of both the prolactin and leptin
475 receptors[62] (Fig.3E). Additionally, these cells have the highest proportion of DVC neuronal
476 co-expression of glutamate and GABA related genes (Fig.3F).
477

478 In our analysis we found a subset of monoaminergic neurons that express the cholecystokinin
479 (*Cck*) gene (Fig.4A). While the *Cck* and *Th*-expressing DVC neurons are considered to be
480 non-overlapping cell types with distinct physiologies[17, 63], we confirmed co-expression of
481 *Th* and *Cck* results by *in-situ* hybridization (Fig.4B). The majority of this overlap occurs in cells
482 belonging to the COE-Atp10a and monoamine class (i.e. M0, M3) cell identities (Fig.4A).
483

484 ### 3.3. The murine DVC cell atlas

485 To generate a comprehensive murine DVC database from multiple datasets, we utilized
486 treeArches[39] to harmonize our snRNA-seq DVC labels with that from a publication by
487 Ludwig and collaborators (i.e. the 'Ludwig dataset')[2] (Fig.5A-B). After building our initial cell
488 hierarchy (Fig.S10), we integrated our dataset with the Ludwig dataset, giving a total of
489 171,868 cells (Fig.5B). Next, the labeled cell identities from the Ludwig dataset[2] were
490 incorporated into our tree based on the similarity between the transcriptomic programs of our
491 labeled identities and the Ludwig-labeled identities using progressive learning through
492 scHPL[41] (Fig.5A). Some of the Ludwig dataset identities failed to be incorporated into our
493 tree, like the oligodendrocyte precursor cells (OPCs), which contain a mix of OPCs and pre-
494 myelinating oligodendrocytes (Fig.S11A). The mix of cell programs makes it impossible for
495 treeArches to correctly add one branch of the Ludwig OPCs to the tree as ideally it would be
496 added as a subpopulation of both the OPCs and pre-myelinating oligodendrocytes, which is
497 not biologically possible. The resultant murine hierarchy has a fourth layer of cellular
498 resolution as some of Ludwig identities, mainly neurons, are subgroups of our cell identities
499 (Fig.S11B).
500

501 We confirmed the validity of our cell hierarchy using three methods. First, by using the learned
502 model to predict the labels of the cells we used to develop them (i.e. this study and the
503 Ludwig dataset), for which we obtained highly concordant cell labeling (Fig.5C). Secondly,
504 we used the learned model to predict the labels of another publicly available dataset from
505 Dowsett and collaborators (i.e. the 'Dowsett dataset')[18] (Fig.5D). Using this approach, we
506 were able to successfully label 95% of these cells at high resolution (i.e. layer 3 or 4 of cell
507 identity granularity); further validating our combined DVC labels. Finally, we manually
508 mapped the marker genes from Ludwig[2] and Dowsett[18] neuronal clusters in our dataset
509 and confirmed the sub-groups of neurons among our identities pointed out by treeArches
510 (Fig.S11B).
511

512 ### 3.4. An integrated rodent DVC cell hierarchy

513 To identify rat DVC cell clusters and subclusters and contrast these with the mouse DVC
514 atlas, we generated a *de novo* ad libitum-fed rat dataset (cells n=12,167) (Fig.6A) and

515 labeled it by mapping the top 5 gene expression markers of each of our murine layer-3 cell
516 identities (Table S8). After manual curation at three granularities (Fig.6B-C; Table S9), we
517 obtained 52 DVC rat identities at high cellular resolution (Fig.6C) including a small group of
518 'unspecific' cells (n=35) that we could not confidently label because its top gene expression
519 markers have unknown functions and none of our known identities' genes clearly marked this
520 population (Fig.6B-C; Table S8).
521
522 We established 10, layer-3 neuronal identities not previously found in the murine data (Fig.6C;
523 Fig.S12A; Table S9). Notably, two of those did not belong to any of the existing murine
524 neuronal classes (i.e. layer-2 of cellular granularity), therefore we created two new layer-2
525 classes (Fig.6B). One of these, the immunity-related neurons, have high cystatin C, *Inpp5d*
526 and *Csf1r* expression, genes commonly associated with immunity-related processes in
527 microglia and with immunomodulation in cancer[64-66] (Fig.7; Table S10). The second neural
528 class identified in rat but not mouse DVC were the 'Pdgfra neurons' (Fig.7). These neurons
529 express *Pdgfra*, *Arhgap31* and *Itga9*, known markers for progenitor cells for which we named
530 this cell class 'ortus-akin' (Latin: 'origin') because they are similar to cells giving origin to other
531 cells[67] (Fig.7A; Table S10). Interestingly, this neuronal class not only expressed *Pdgfra*,
532 but also other OPC signature genes (Fig.7A). Mapping the expression levels of metabolic-
533 associated receptors revealed that both immunity-akin and ortus-akin express GFRAL,
534 prolactin receptor and leptin receptor (Fig.7B), although they seem to have a varied
535 neurotransmitter profile (Fig.S12B). To confirm the presence of *Pdgfra*-expressing neurons in
536 the rat DVC, we performed immunostaining in the mouse and rat brainstem. Within the mouse,
537 we found PDGFRA-immunoreactivity(IR) in the two morphologically distinct cells; matching
538 OPC and blood vessel-associated fibroblast morphologies(Fig.7C). However, within the rat,
539 we identified PDGFRA-IR in cells with three morphologies, one of which resembled neurons
540 with an enlarged cell body and protruding cellular processes (Fig.7C). To determine if these
541 PDGFRA-IR cells were neurons, we co-stained with the neural marker, HuC/D and noted
542 several PDGFRA and HuC/D copositive cells (Fig.7D); confirming our sequencing data that
543 a PDGFRA-expressing neural class exists in the rat DVC and localizing these cells to the area
544 postrema.
545
546 To construct an integrated rodent DVC cell atlas, we incorporated the labeled rat dataset into
547 our hierarchy using treeArches[39] (Fig.8). The rodent data was projected onto the mouse
548 datasets (Fig.8A) and the 42 high resolution rat cell identities were appended to the tree
549 (Fig.8B; Fig.S13). The final hierarchy has 123 labels of which 99 are high resolution according
550 to our cellular granularity (i.e. layers 3 to 5) (Fig.8B). In addition it has 20 layer-2 identities
551 and 7 cell identities that are novel from the rat dataset (Fig.8B).

552
553 ### 3.5. *Hcrt* and *Agrp* expression in the DVC
554 Since *Agrp*-expressing cells have been recently described within the DVC[68], we mapped
555 this and other neuropeptide genes in DVC neurons. Surprisingly, we found *Hcrt* and *Agrp*
556 mRNA in neurons in our dataset (Fig.S14A). We then performed *in-situ* hybridizations for
557 these transcripts in both the mouse hypothalamus and DVC. While both *Hcrt* and *Agrp* were
558 readily detectable in the hypothalamus, we failed to observe signal within the DVC (Fig.S14B).
559 Since we also found expression of *Hcrt* and *Agrp* in neurons of the Dowsett and Ludwig
560 datasets[2, 18] (Fig.S14C), we then mapped the sequenced reads from these transcripts and
561 confirmed that most of them mapped to intronic and non-coding regions of these genes
562 (Fig.S14D). Furthermore, our rat DVC dataset was pre-processed excluding introns from the
563 reads mapping, and the *Hcrt* and *Agrp* expression levels observed is minimal (Fig.S14E),
564 which is in agreement with the non-coding location of the reads in mouse DVC. These data
565 explain absence of signal from our *in-situ* hybridizations and suggests DVC cells do not
566 produce HCRT or AGRP neuropeptides.
567
568 ### 3.6. Meal-related transcriptional programs in the murine DVC
569 As the DVC acts as a primary node for meal-related signals[69], we wanted to define which
570 of our cell identities responded to meal consumption and thus performed differential gene
571 expression analysis between DVC cell types from mice that were euthanized under fasting
572 conditions, with ad libitum access to food or two hours post-refeeding following an overnight
573 fast (Fig.1A; Fig.9). This analysis revealed widespread transcriptional changes across nearly
574 every neural cell identity, the exceptions being corelautus, Golli class and pH classes
575 (Fig.9A). Additionally, the size of the transcriptional changes were relatively small, with
576 approximately 90% of the differentially expressed genes having increases or decreases
577 between 0.5 and 1.0 log2 fold-change, with only ~10% of the gene changes being ≥1 log2
578 fold-change between conditions (Fig.9A). Of the responding neurons, magnaclasses 1 and
579 2, which represent large populations of predominately inhibitory and excitatory neurons
580 (Fig.S2), showed the greatest number of differentially expressed genes following refeeding
581 for both comparisons refed versus fasting, and refed versus ad libitum food access (Fig.9A).
582 To understand how refeeding transcriptionally alters inhibitory compared with excitatory DVC
583 neurons, we compared differentially expressed genes between these two classes across
584 conditions. Intriguingly, despite being in transcriptionally distinct classes, we found meal
585 consumption altered many of the same genes (Fig.9B-D), suggesting these cells may be
586 receiving similar postprandial signals which are propagated via these cells in unique
587 manners. This is supported by the similar receptor expression profile of magnaclass 1 and 2
588 (Fig.S15). One notable exception is *Cckbr* which is upregulated in magnaclass 2 and

589 downregulated in magnaclass 1 in refeeding when compared with ad libitum fed mice(**Table**
590 **S12**). We also note that oligodendrocytes contained the highest number of differentially
591 expressed genes in refeeding (**Fig.9A**). While the roles of oligodendrocytes in refeeding
592 responses within the DVC have yet to be determined and the biologic significance of these
593 changes are presently unclear, DVC oligodendrocytes also have robust transcriptional
594 responses in response to fasting[18]; suggesting these cells are sensitive to both positive
595 and negative energy balance associated-cues and may have important roles in regulating
596 energy homeostasis..
597
598 ## 4. Discussion
599 The recent success of DVC-based therapies[12, 70] has moved DVC biology to the forefront
600 of weight control therapies and there is now clear clinical impetus to fully define DVC cell
601 types and their functions. Previous studies detailing DVC cell types describe a high degree
602 of heterogeneity[2, 18, 19], however, these studies lacked an in-depth analysis of
603 neurotransmitter profiles of neurons, any cross-species evaluation of DVC cell types, or an
604 analysis of how meal consumption transcriptionally regulates these cells. We therefore
605 developed *de novo* mouse and rat DVC cell atlases to address these points.
606
607 To more fully describe the cellular complexity within the DVC, we combined a pipeline of cell
608 label transfer using brain existing published datasets and thorough curation of cell identities,
609 which resulted in a 4-layer mouse cell hierarchy and a 5-layer rodent cell hierarchy of the
610 DVC. Within this hierarchy we found several unique features of DVC glial cells. First, we found
611 highly excitable Ca^+-permeable astrocytes in the DVC in which *Gfap* is almost exclusively
612 expressed and they coexpress *Kcnj3* (GIRK1 potassium channel). These cells largely lack
613 *Gria2*, consistent with findings in Bergmann glial cells in which colocalization of *Gria2* and
614 GFAP was found to alter neuron-glial interactions[71]. Comparing Ca^+-permeable DVC
615 astrocytes to hypothalamic astrocytes[43], we found the same expression pattern with
616 minimal overlap between *Gria2* and *Gfap.* However, DVC astrocytes seem to have some
617 unique properties when compared with hypothalamic, cortical and hippocampal astrocytes.
618 Principally DVC astrocytes express the GIRK1 channel, likely rendering them more excitable.
619 Additionally, while we identified hypothalamic fibroblasts which express high *Aldh1a1* similar
620 to the DVC p-fibroblasts, we failed to find a group equivalent to s-fibroblasts. Other cell
621 populations seem to be consistent to what has been found in other brain sites, like the
622 intermediate oligodendrocytes that are found enriched in the hypothalamus and the corpus
623 callosum in mice[55]. In summary, these findings show certain DVC glial cells share identities
624 with glial cells from other CNS sites, there are DVC-specific glial cells.
625

626 Within the mouse neural classes, we found overlap between *Cck* and *Th*-expressing cells. As
627 these cells have previously been described as non-overlapping, this was unexpected[17].
628 Our *in-situ* hybridization confirmed the presence of *Cck*/*Th* positive cells within the NTS and
629 AP. We believe the discrepancy may be due to detection methods as these cells were initially
630 defined as non-overlapping using immunofluorescent detection of TH protein and a *Cck*
631 genetic reporter[17]. Functional studies of *Cck*- and *Th*-expressing neurons within the NTS
632 demonstrate these cells have somewhat distinct roles; while both reduce appetite, *Cck*
633 neurons are strongly aversive whereas *Th*-labelled neurons are non-aversive[72]. While no
634 functional characterization of *Cck* and *Th* neurons of the AP has been performed, we posit
635 that as some *Th*-expressing AP neurons also express *Gfral* and *Casr*; both having potently
636 aversive ligands (e.g. GDF15, deoxynivalenol)[16, 73]; they are likely to mediate aversive
637 anorexia. The role of dual *Cck/Th* positive neurons remains to be determined.
638
639 While AGRP expression has long been considered to be hypothalamic-exclusive, a recent
640 report describes *Agrp*-expressing cells within the mouse DVC[68], i n part from the detection
641 of Agrp mRNA in scRNA-Seq data. Similarly, we also detected transcripts for both *Agrp* and
642 *Hcrt* in our snRNA-Seq data but failed to detect any transcripts within the DVC by *in-situ*
643 hybridizations. One possible explanation for the discrepancy between the snRNA-Seq data
644 and our *in-situ* hybridizations data is that the snRNA-Seq mRNA reads for *Agrp* and *Hcrt* gene
645 overwhelmingly mapped to non-coding regions, of the respective genes. Combined, these
646 data suggests to us that neither AGRP or HCRT neuropeptides are produced by DVC cells
647 in rodents.
648
649 We show the presence of neurons with seemingly mixed programs in the DVC, which we
650 called 'mixed neurons'. Similar groups have been described in the hypothalamus[26]
651 suggesting that some neurons may have hybrid-functionalities. These mixed neurons share
652 many transcriptomic markers expression with many other cell identities, and may require the
653 use of other technologies to fully identify them anatomically in the brain.
654
655 To perform a cross-species analysis, we generated a rat-based DVC atlas and compared it
656 with the mouse DVC. Our rat dataset was smaller than the mouse data, it is possible some of
657 the of the new neuronal cell identities (e.g. M_sema, M4) may contain cells belonging to
658 multiple cell types, as treeArches did not appended these identities to the tree. Despite this,
659 we corroborated two new cell types in the rat DVC that are not present in mice the *Pdgfa*-
660 expressing (ortus-akin class) and the immunity-related neurons. *Pdgfra* is a well described
661 marker gene for OPCs and fibroblasts within the central nervous system[67] but, to our
662 knowledge, has not been associated with neurons. Notably, although the PDGFRA immuno-

signal in HuC/D+ neurons is clearly discernible, it is less intense than in OPCs and fibroblasts, in agreement with expression levels from our snRNA-Seq data. Since it was previously demonstrated that OPCs can give rise to neurons in the adult brain[74] and there is evidence of neurogenesis in the AP following amylin administration in rats[75], it is possible that these PDGFRA+/HuCD+ cells in the AP represent a transient stage of PDGFRA+ OPCs differentiating into neurons.

Regardless of their maturity, we speculate that the Pdgfra neurons (ortus-akin class) have roles in appetite regulation as they express leptin receptor and *Gfral*. Interestingly, while multiple studies have failed to detect *Lepr* via Cre-based reporters[62, 76] or leptin-induced phosphorylated STAT3 in the AP of mice[77], *Lepr* and leptin-induced phosphorylated STAT3 are detectable within the rat AP[78-80]. We believe one explanation for this species discrepancy in *Lepr* expression is the absence of the ortus class neurons in mice. Future studies are needed to characterize these cells and determine whether their presence is found in other mammals including humans.

DVC-targeting obesity therapeutics, including amylin and GLP1 mimetics, produce clinically relevant weight loss but are associated with multiple gastrointestinal adverse events and there is a need to develop new obesity therapies that can reduce appetite without unwanted gastrointestinal side effects[81, 82]. Indeed, the DVC cells that regulate appetite suppression and nausea are separable[72], making targeting such cells an attractive target for pharmacotherapy. As meal consumption is generally not associated with gastrointestinal distress, we sought to identify refeeding responsive cells within the mouse DVC. From this analysis, we found nearly all neural cell identities are transcriptionally altered by meal consumption. We also found the magnitude of transcriptional changes was relatively small, regardless of the cell class examined. While relatively small, the scale of the transcriptional changes in response to refeeding are similar to many of the gene expression changes observed in *Agrp*-neurons following 16 hours food deprivation[43]. Regardless of whether this is a technical limitation of snRNA-Seq methods or accurately reflects the scale of transcriptional changes in the DVC, utilizing Therefore, identifying neurons that promote non-aversive anorexia via the transcriptional response to refeeding to identify neural classes as targets for as the basis of pharmacotherapy is unlikely to yield specific and targetable pathways.

In general, one limitation in our study is that it is based on nuclear RNA which may reflect a fraction of biological changes. Using nuclear isolation facilitates generating to have single-neuron data[83] since obtaining viable whole neurons (including all their processes) is very

challenging. Previous studies on the relationship between nuclear and cellular RNA content in brain show that nuclear sequencing reads may map to intronic regions of genes in higher proportion[84]. Although this does not appear to impact gene expression analysis for neurons in the current pipelines like the ones we used for our mouse data[84, 85], it is possible that some biological features such as microglial activation state, are not fully recovered using nuclear RNA[86]. Although we performed sub-clustering in the mouse microgia and assessment of the resulting marker genes for each group, we did not find evidence of activation possibly due to this matter. Separately, for meal consumption, we were unable to analyze responses in individual mice as pooling DVCs from individual mice was the most amenable option to maximize nuclei for in our pipeline. As we pooled DVCs from both sexes, this limited our ability to detect sexual dimorphic cell class proportions and gene expression levels.

5. Conclusion

As the amount of snRNA-Seq data performed on the DVC continues to grow, there is a need for a common, scalable label set that can be applied to new studies and integrate new sequencing data. To develop such a label set, we started with a *de novo* DVC atlas, we generated three layers of cellular granularity for both neural and non-neuronal cell types. Then, using the treeArches pipeline[39] we harmonized our snRNA-Seq labels with the Ludwig dataset[2] and increased our cellular granularity from three to four layers of resolution. Manually curating and harmonizing our dataset enhanced the ability of our cell atlas to capture the complexity of the DVC neurons since not all groups seem to contain easily delineable subgroups of cells. For example, eleven of the labels incorporated into our cell hierarchy in this pipeline belong to the monoaminergic neuronal class, which seem to encompass multiple subgroups of specialized cells. We further constructed the rodent DVC cell atlas which resulted in a fifth layer of cell identity to the monoaminergic M3 neurons. Although the number of identities increases as layers are more specific, this gives this unified atlas greater adaptability to different research needs. Additionally, our labels can be accurately harmonized with new databases regardless of size and new DVC snRNA-Seq data can be added to the tree to generate new branches. Thus, our unified rodent DVC atlas is highly amenable to future research elucidating new biologic and therapeutic insights into DVC cell types.

6. Acknowledgements

We would like to thank authors of the Ludwig and the Dowsett publications for making publicly available their datasets. We thank M. Myers Jr. for the valuable help provided; S. Hebert and S. Bailey for their insights and suggestions in regards to the bioinformatic analysis; members

of the Kokoeva lab for their insights on the *in-situ* hybridization and immunohistochemistry pipelines; S. Feng and M. Fu for technical assistance for images acquisition at the Molecular Imaging Platform at the RI-MUHC, and A. Duensing for assistance with relevant file transfer.

7. Author contributions

Conceptualization: CH and PS
Methodology: CH, AB, LM, MK and PS
Sample collection: AB and PS
Software: CH, LM and HJM
Data analysis: CH, LM, MK and PS
Data curation: CH and HJM
Validation of findings: CH, FS, HJM and PS
Imaging: CH and PS
Visualization: CH, MK and PS
Supervision: CH and PS
Writing—original draft: CH and PS —review and editing: CH, AB, LM, FS, HJM, MK and PS
Funding acquisition: MK and PS

8. Funding

This research was also supported by grants from Canadian Institutes for Health Research (PJT180590 for PVS and 202010PJT for MK) the Natural Sciences and Engineering Research Council of Canada (RGPIN-2022-03390). HJM was funded in part by the Canada First Research Excellence Fund and Fonds de recherche du Quebec, awarded to the Healthy Brains, Healthy Lives initiative.

9. Declaration of interests

The authors declare that they have no competing interests.

10. Data statement

All data needed to evaluate the conclusions in the paper are present in the paper and/or the Supplementary Materials. FASTQ files have been deposited in the NCBI Sequence Read Archive (Accession: PRJNA1161292). In addition, our murine and rat datasets have been made available for visualization and analysis through the Broad Institute Single Cell Portal (https://singlecell.broadinstitute.org/single_cell/study/SCP2773). The labels from our cell atlas can be transferred to new datasets through treeArches using the available hosted Jupyter Notebook in Google Colab for the mouse data (https://colab.research.google.com/drive/1v983gcQxIwBN-

774 4lGx18JXPweZoKqMbwX#scrollTo=SJTZppZWa-63), and for the rodent data
775 (https://colab.research.google.com/drive/10tAmfRosMscuBak6wHX80TgdEBsHeWQB#scro
776 llTo=941ab5c1-8910-4e67-a632-4d18601d45b4). Original code used for constructing the
777 murine and rodent cell hierarchies and predicting labels using treeArches are available in
778 the GitHub repository https://github.com/LabSabatini/DVC_cell_atlas.
779

References

[1] L. Gautron, J.K. Elmquist, K.W. Williams, Neural control of energy balance: translating circuits to therapies, Cell. 161 (2015) 133-45. 10.1016/j.cell.2015.02.023.

[2] M.Q. Ludwig, W. Cheng, D. Gordian, J. Lee, S.J. Paulsen, S.N. Hansen, et al., A genetic map of the mouse dorsal vagal complex and its role in obesity, Nat Metab. 3 (2021) 530-45. 10.1038/s42255-021-00363-1.

[3] L. Bai, S. Mesgarzadeh, K.S. Ramesh, E.L. Huey, Y. Liu, L.A. Gray, et al., Genetic Identification of Vagal Sensory Neurons That Control Feeding, Cell. 179 (2019) 1129-43 e23. 10.1016/j.cell.2019.10.031.

[4] W. Han, L.A. Tellez, M.H. Perkins, I.O. Perez, T. Qu, J. Ferreira, et al., A Neural Circuit for Gut-Induced Reward, Cell. 175 (2018) 665-78 e23. 10.1016/j.cell.2018.08.049.

[5] E.K. Williams, R.B. Chang, D.E. Strochlic, B.D. Umans, B.B. Lowell, S.D. Liberles, Sensory Neurons that Detect Stretch and Nutrients in the Digestive System, Cell. 166 (2016) 209-21. 10.1016/j.cell.2016.05.011.

[6] M.W. Schwartz, Central nervous system regulation of food intake, Obesity (Silver Spring). 14 Suppl 1 (2006) 1S-8S. 10.1038/oby.2006.275.

[7] W. Cheng, E. Ndoka, J.N. Maung, W. Pan, A.C. Rupp, C.J. Rhodes, et al., NTS Prlh overcomes orexigenic stimuli and ameliorates dietary and genetic forms of obesity, Nat Commun. 12 (2021) 5175. 10.1038/s41467-021-25525-3.

[8] W. Qiu, C.R. Hutch, Y. Wang, J. Wloszek, R.A. Rucker, M.G. Myers, et al., Multiple NTS neuron populations cumulatively suppress food intake, Elife. 12 (2023) 10.7554/eLife.85640.

[9] T. Borner, C.G. Liberini, T.A. Lutz, T. Riediger, Brainstem GLP-1 signalling contributes to cancer anorexia-cachexia syndrome in the rat, Neuropharmacology. 131 (2018) 282-90. 10.1016/j.neuropharm.2017.12.024.

[10] C.W. le Roux, O. Steen, K.J. Lucas, E. Startseva, A. Unseld, A.M. Hennige, Glucagon and GLP-1 receptor dual agonist survodutide for obesity: a randomised, double-blind, placebo-controlled, dose-finding phase 2 trial, Lancet Diabetes Endocrinol. 12 (2024) 162-73. 10.1016/S2213-8587(23)00356-X.

[11] S.M. Advani, P.G. Advani, H.M. VonVille, S.H. Jafri, Pharmacological management of cachexia in adult cancer patients: a systematic review of clinical trials, BMC Cancer. 18 (2018) 1174. 10.1186/s12885-018-5080-4.

[12] M.M. Veniant, S.C. Lu, L. Atangan, R. Komorowski, S. Stanislaus, Y. Cheng, et al., A GIPR antagonist conjugated to GLP-1 analogues promotes weight loss with improved metabolic parameters in preclinical and phase 1 settings, Nat Metab. 6 (2024) 290-303. 10.1038/s42255-023-00966-w.

[13] J.M. Adams, H. Pei, D.A. Sandoval, R.J. Seeley, R.B. Chang, S.D. Liberles, et al., Liraglutide Modulates Appetite and Body Weight Through Glucagon-Like Peptide 1 Receptor-Expressing Glutamatergic Neurons, Diabetes. 67 (2018) 1538-48. 10.2337/db17-1385.

[14] K.P. Huang, A.A. Acosta, M.Y. Ghidewon, A.D. McKnight, M.S. Almeida, N.T. Nyema, et al., Dissociable hindbrain GLP1R circuits for satiety and aversion, Nature. 632 (2024) 585-93. 10.1038/s41586-024-07685-6.

[15] I. Medic, S. Gulati, H.-J. Lenz, D. Mahalingam, J. Thomas, J. Luo, et al., Initial results of a cohort of advanced prostate cancer patients in a phase Ia study of NGM120, a first-in-class anti- GDNF family receptor alpha like (GFRAL) antibody, Annals of Oncology. 33 (2022) S1186-S. 10.1016/j.annonc.2022.07.1888.

[16] L. Yang, C.C. Chang, Z. Sun, D. Madsen, H. Zhu, S.B. Padkjaer, et al., GFRAL is the receptor for GDF15 and is required for the anti-obesity effects of the ligand, Nat Med. 23 (2017) 1158-66. https://doi.org/10.1038/nm.4394.

[17] C.W. Roman, V.A. Derkach, R.D. Palmiter, Genetically and functionally defined NTS to PBN brain circuits mediating anorexia, Nat Commun. 7 (2016) 11905. 10.1038/ncomms11905.

[18] G.K.C. Dowsett, B.Y.H. Lam, J.A. Tadross, I. Cimino, D. Rimmington, A.P. Coll, et al., A survey of the mouse hindbrain in the fed and fasted states using single-nucleus RNA sequencing, Mol Metab. 53 (2021) 101240. 10.1016/j.molmet.2021.101240.
[19] C. Zhang, J.A. Kaye, Z. Cai, Y. Wang, S.L. Prescott, S.D. Liberles, Area Postrema Cell Types that Mediate Nausea-Associated Behaviors, Neuron. 109 (2021) 461-72 e5. 10.1016/j.neuron.2020.11.010.
[20] S.M. Fortin, R.K. Lipsky, R. Lhamo, J. Chen, E. Kim, T. Borner, et al., GABA neurons in the nucleus tractus solitarius express GLP-1 receptors and mediate anorectic effects of liraglutide in rats, Sci Transl Med. 12 (2020) 10.1126/scitranslmed.aay8071.
[21] G.X. Zheng, J.M. Terry, P. Belgrader, P. Ryvkin, Z.W. Bent, R. Wilson, et al., Massively parallel digital transcriptional profiling of single cells, Nat Commun. 8 (2017) 14049. 10.1038/ncomms14049.
[22] R.C. Team. R: A Language and Environment for Statistical Computing. Vienna, Austria: R Foundation for Statistical Computing; 2023.
[23] Y. Hao, T. Stuart, M.H. Kowalski, S. Choudhary, P. Hoffman, A. Hartman, et al., Dictionary learning for integrative, multimodal and scalable single-cell analysis, Nat Biotechnol. 42 (2024) 293-304. 10.1038/s41587-023-01767-y.
[24] C.S. McGinnis, L.M. Murrow, Z.J. Gartner, DoubletFinder: Doublet Detection in Single-Cell RNA Sequencing Data Using Artificial Nearest Neighbors, Cell Syst. 8 (2019) 329-37 e4. 10.1016/j.cels.2019.03.003.
[25] I. Korsunsky, N. Millard, J. Fan, K. Slowikowski, F. Zhang, K. Wei, et al., Fast, sensitive and accurate integration of single-cell data with Harmony, Nat Methods. 16 (2019) 1289-96. https://doi.org/10.1038/s41592-019-0619-0.
[26] J.N. Campbell, E.Z. Macosko, H. Fenselau, T.H. Pers, A. Lyubetskaya, D. Tenen, et al., A molecular census of arcuate hypothalamus and median eminence cell types, Nat Neurosci. 20 (2017) 484-96. 10.1038/nn.4495.
[27] R. Chen, X. Wu, L. Jiang, Y. Zhang, Single-Cell RNA-Seq Reveals Hypothalamic Cell Diversity, Cell Rep. 18 (2017) 3227-41. 10.1016/j.celrep.2017.03.004.
[28] R.A. Romanov, A. Zeisel, J. Bakker, F. Girach, A. Hellysaz, R. Tomer, et al., Molecular interrogation of hypothalamic organization reveals distinct dopamine neuronal subtypes, Nat Neurosci. 20 (2017) 176-88. 10.1038/nn.4462.
[29] B. Tasic, V. Menon, T.N. Nguyen, T.K. Kim, T. Jarsky, Z. Yao, et al., Adult mouse cortical cell taxonomy revealed by single cell transcriptomics, Nat Neurosci. 19 (2016) 335-46. 10.1038/nn.4216.
[30] D. Aran, A.P. Looney, L. Liu, E. Wu, V. Fong, A. Hsu, et al., Reference-based analysis of lung single-cell sequencing reveals a transitional profibrotic macrophage, Nat Immunol. 20 (2019) 163-72. https://doi.org/10.1038/s41590-018-0276-y.
[31] D. Risso, M. Cole. scRNAseq: Collection of Public Single-Cell RNA-Seq Datasets. 2.16.0 ed2023.
[32] G. Finak, A. McDavid, M. Yajima, J. Deng, V. Gersuk, A.K. Shalek, et al., MAST: a flexible statistical framework for assessing transcriptional changes and characterizing heterogeneity in single-cell RNA sequencing data, Genome Biol. 16 (2015) 278. 10.1186/s13059-015-0844-5.
[33] R. Cannoodt, W. Saelens, D. Sichien, S. Tavernier, S. Janssens, M. Guilliams, et al., SCORPIUS improves trajectory inference and identifies novel modules in dendritic cell development., Preprint at bioRxiv. (2016) https://doi.org/10.1101/079509.
[34] K. Ushey, J. Allaire, Y. Tang. reticulate: Interface to 'Python'. 1.35.0 ed2024.
[35] R. Cannoodt. anndata: 'anndata' for R. 0.7.5.6 ed2023.
[36] G. Van Rossum, F.L. Drake. Python 3 Reference Manual. 3.9 ed. Scotts Valley, CA: CreateSpace; 2009.
[37] A. Sathyamurthy, K.R. Johnson, K.J.E. Matson, C.I. Dobrott, L. Li, A.R. Ryba, et al., Massively Parallel Single Nucleus Transcriptional Profiling Defines Spinal Cord Neurons and Their Activity during Behavior, Cell Rep. 22 (2018) 2216-25. 10.1016/j.celrep.2018.02.003.
[38] M.Y. Batiuk, A. Martirosyan, J. Wahis, F. de Vin, C. Marneffe, C. Kusserow, et al., Identification of region-specific astrocyte subtypes at single cell resolution, Nat Commun. 11 (2020) 1220. 10.1038/s41467-019-14198-8.

[39] L. Michielsen, M. Lotfollahi, D. Strobl, L. Sikkema, M.J.T. Reinders, F.J. Theis, et al., Single-cell reference mapping to construct and extend cell-type hierarchies, NAR Genom Bioinform. 5 (2023) lqad070. 10.1093/nargab/lqad070.
[40] A. Gayoso, R. Lopez, G. Xing, P. Boyeau, V. Valiollah Pour Amiri, J. Hong, et al., A Python library for probabilistic analysis of single-cell omics data, Nat Biotechnol. 40 (2022) 163-6. 10.1038/s41587-021-01206-w.
[41] L. Michielsen, M.J.T. Reinders, A. Mahfouz, Hierarchical progressive learning of cell identities in single-cell data, Nat Commun. 12 (2021) 2799. 10.1038/s41467-021-23196-8.
[42] J.D. Hunter, Matplotlib: A 2D graphics environment, Computing in Science & Engineering. 3 (2007) 90-5. 10.1109/MCSE.2007.55.
[43] L. Steuernagel, B.Y.H. Lam, P. Klemm, G.K.C. Dowsett, C.A. Bauder, J.A. Tadross, et al., HypoMap-a unified single-cell gene expression atlas of the murine hypothalamus, Nat Metab. 4 (2022) 1402-19. 10.1038/s42255-022-00657-y.
[44] S. Jessa, A. Blanchet-Cohen, B. Krug, M. Vladoiu, M. Coutelier, D. Faury, et al., Stalled developmental programs at the root of pediatric brain tumors, Nat Genet. 51 (2019) 1702-13. 10.1038/s41588-019-0531-7.
[45] C.E. Vaaga, M. Borisovska, G.L. Westbrook, Dual-transmitter neurons: functional implications of co-release and co-transmission, Curr Opin Neurobiol. 29 (2014) 25-32. 10.1016/j.conb.2014.04.010.
[46] N.X. Tritsch, A.J. Granger, B.L. Sabatini, Mechanisms and functions of GABA co-release, Nat Rev Neurosci. 17 (2016) 139-45. 10.1038/nrn.2015.21.
[47] C.F. Landry, J.A. Ellison, T.M. Pribyl, C. Campagnoni, K. Kampf, A.T. Campagnoni, Myelin basic protein gene expression in neurons: developmental and regional changes in protein targeting within neuronal nuclei, cell bodies, and processes., J Neurosci. 16 (1996) 2452-62. 10.1523/JNEUROSCI.16-08-02452.1996.
[48] D. Lutz, G. Loers, R. Kleene, I. Oezen, H. Kataria, N. Katagihallimath, et al., Myelin basic protein cleaves cell adhesion molecule L1 and promotes neuritogenesis and cell survival, J Biol Chem. 289 (2014) 13503-18. 10.1074/jbc.M113.530238.
[49] V.T. Cheli, D.A. Santiago Gonzalez, V. Spreuer, V. Handley, A.T. Campagnoni, P.M. Paez, Golli Myelin Basic Proteins Modulate Voltage-Operated Ca(++) Influx and Development in Cortical and Hippocampal Neurons, Mol Neurobiol. 53 (2016) 5749-71. 10.1007/s12035-015-9499-1.
[50] M. Melone, S. Ciappelloni, F. Conti, Plasma membrane transporters GAT-1 and GAT-3 contribute to heterogeneity of GABAergic synapses in neocortex, Front Neuroanat. 8 (2014) 72. 10.3389/fnana.2014.00072.
[51] S.M. Theparambil, P.S. Hosford, I. Ruminot, O. Kopach, J.R. Reynolds, P.Y. Sandoval, et al., Astrocytes regulate brain extracellular pH via a neuronal activity-dependent bicarbonate shuttle, Nat Commun. 11 (2020) 5073. 10.1038/s41467-020-18756-3.
[52] Y. Kubo, T.J. Baldwin, Y.N. Jan, L.Y. Jan, Primary structure and functional expression of a mouse inward rectifier potassium channel, Nature. 362 (1993) 127–33. https://doi.org/10.1038/362127a0.
[53] N. Burnashev, A. Khodorova, P. Jonas, P.J. Helm, W. Wisden, H. Monyer, et al., Calcium-Permeable AMPA-Kainate Receptors in Fusiform Cerebellar Glial Cells, Science. 256 (1992) 1566-70. http://dx.doi.org/10.1126/science.1317970.
[54] J.R.P. Geiger, T. Melcher, D.S. Koh, B. Sakmann, S.P. H., P. Jonas, et al., Relative Abundance of Subunit mRNAs Determines Gating and Ca*+ Permeability of AMPA Receptors in Principal Neurons and Interneurons in Rat CNS, Neuron. 15 (1995) 193-204. doi:10.1016/0896-6273(95)90076-4.
[55] S. Marques, A. Zeisel, S. Codeluppi, D. van Bruggen, A. Mendanha Falcao, L. Xiao, et al., Oligodendrocyte heterogeneity in the mouse juvenile and adult central nervous system, Science. 352 (2016) 1326-9. 10.1126/science.aaf6463.
[56] M. Kasai, Y. Omae, Y. Kawai, A. Shibata, A. Hoshino, M. Mizuguchi, et al., GWAS identifies candidate susceptibility loci and microRNA biomarkers for acute encephalopathy with biphasic seizures and late reduced diffusion, Sci Rep. 12 (2022) 1332. 10.1038/s41598-021-04576-y.

[57] A.B. DePaula-Silva, C. Gorbea, D.J. Doty, J.E. Libbey, J.M.S. Sanchez, T.J. Hanak, et al., Differential transcriptional profiles identify microglial- and macrophage-specific gene markers expressed during virus-induced neuroinflammation, J Neuroinflammation. 16 (2019) 152. 10.1186/s12974-019-1545-x.
[58] N. Koutsodendris, J. Blumenfeld, A. Agrawal, M. Traglia, B. Grone, M. Zilberter, et al., Neuronal APOE4 removal protects against tau-mediated gliosis, neurodegeneration and myelin deficits, Nat Aging. 3 (2023) 275-96. 10.1038/s43587-023-00368-3.
[59] L. Schirmer, D. Velmeshev, S. Holmqvist, M. Kaufmann, S. Werneburg, D. Jung, et al., Neuronal vulnerability and multilineage diversity in multiple sclerosis, Nature. 573 (2019) 75-82. 10.1038/s41586-019-1404-z.
[60] J. Creus-Muncunill, J.V. Haure-Mirande, D. Mattei, J. Bons, A.V. Ramirez, B.W. Hamilton, et al., TYROBP/DAP12 knockout in Huntington's disease Q175 mice cell-autonomously decreases microglial expression of disease-associated genes and non-cell-autonomously mitigates astrogliosis and motor deterioration, J Neuroinflammation. 21 (2024) 66. 10.1186/s12974-024-03052-4.
[61] L.L. Tang, Y.B. Wu, C.Q. Fang, P. Qu, Z.L. Gao, NDRG2 promoted secreted miR-375 in microvesicles shed from M1 microglia, which induced neuron damage, Biochem Biophys Res Commun. 469 (2016) 392-8. 10.1016/j.bbrc.2015.11.098.
[62] W. Cheng, E. Ndoka, C. Hutch, K. Roelofs, A. MacKinnon, B. Khoury, et al., Leptin receptor-expressing nucleus tractus solitarius neurons suppress food intake independently of GLP1 in mice, JCI Insight. 5 (2020) 10.1172/jci.insight.134359.
[63] C.W. Roman, S.R. Sloat, R.D. Palmiter, A tale of two circuits: CCK(NTS) neuron stimulation controls appetite and induces opposing motivational states by projections to distinct brain regions, Neuroscience. 358 (2017) 316-24. 10.1016/j.neuroscience.2017.06.049.
[64] V. Chou, R.V. Pearse, 2nd, A.J. Aylward, N. Ashour, M. Taga, G. Terzioglu, et al., INPP5D regulates inflammasome activation in human microglia, Nat Commun. 14 (2023) 7552. 10.1038/s41467-023-42819-w.
[65] S.O. Kleeman, T.M. Thakir, B. Demestichas, N. Mourikis, D. Loiero, M. Ferrer, et al., Cystatin C is glucocorticoid responsive, directs recruitment of Trem2+ macrophages, and predicts failure of cancer immunotherapy, Cell Genom. 3 (2023) 100347. 10.1016/j.xgen.2023.100347.
[66] N. Hagan, J.L. Kane, D. Grover, L. Woodworth, C. Madore, J. Saleh, et al., CSF1R signaling is a regulator of pathogenesis in progressive MS, Cell Death Dis. 11 (2020) 904. 10.1038/s41419-020-03084-7.
[67] S.H. Kang, M. Fukaya, J.K. Yang, J.D. Rothstein, D.E. Bergles, NG2+ CNS glial progenitors remain committed to the oligodendrocyte lineage in postnatal life and following neurodegeneration, Neuron. 68 (2010) 668-81. 10.1016/j.neuron.2010.09.009.
[68] T.P. Bachor, E. Hwang, E. Yulyaningsih, K. Attal, F. Mifsud, V. Pham, et al., Identification of AgRP cells in the murine hindbrain that drive feeding, Mol Metab. 80 (2024) 101886. 10.1016/j.molmet.2024.101886.
[69] M.K. Holt, The ins and outs of the caudal nucleus of the solitary tract: An overview of cellular populations and anatomical connections, J Neuroendocrinol. 34 (2022) e13132. 10.1111/jne.13132.
[70] D.M. Breen, H. Kim, D. Bennett, R.A. Calle, S. Collins, R.M. Esquejo, et al., GDF-15 Neutralization Alleviates Platinum-Based Chemotherapy-Induced Emesis, Anorexia, and Weight Loss in Mice and Nonhuman Primates, Cell Metab. 32 (2020) 938-50 e6. 10.1016/j.cmet.2020.10.023.
[71] K. Tsuzuki, S. Ishiuchi, GluR2 expressed by glial fibrillary acidic protein promoter decreases the number of neurons, Front Biosci (Landmark Ed). 13 (2008) 2784–96. https://doi.org/10.2741/2885.
[72] W. Cheng, I. Gonzalez, W. Pan, A.H. Tsang, J. Adams, E. Ndoka, et al., Calcitonin Receptor Neurons in the Mouse Nucleus Tractus Solitarius Control Energy Balance via the Non-aversive Suppression of Feeding, Cell Metab. 31 (2020) 301-12 e5. 10.1016/j.cmet.2019.12.012.

[73] A.R. Patel, H. Frikke-Schmidt, P.V. Sabatini, A.C. Rupp, D.A. Sandoval, M.G. Myers, Jr., et al., Neither GLP-1 receptors nor GFRAL neurons are required for aversive or anorectic response to DON (vomitoxin), Am J Physiol Regul Integr Comp Physiol. 324 (2023) R635-44. 10.1152/ajpregu.00189.2022.
[74] S.C. Robins, E. Trudel, O. Rotondi, X. Liu, T. Djogo, D. Kryzskaya, et al., Evidence for NG2-glia derived, adult-born functional neurons in the hypothalamus, PLoS One. 8 (2013) e78236. 10.1371/journal.pone.0078236.
[75] C.G. Liberini, T. Borner, C.N. Boyle, T.A. Lutz, The satiating hormone amylin enhances neurogenesis in the area postrema of adult rats, Mol Metab. 5 (2016) 834-43. 10.1016/j.molmet.2016.06.015.
[76] N. Wada, S. Hirako, F. Takenoya, H. Kageyama, M. Okabe, S. Shioda, Leptin and its receptors, J Chem Neuroanat. 61-62 (2014) 191-9. 10.1016/j.jchemneu.2014.09.002.
[77] H. Munzberg, J.S. Flier, C. Bjorbaek, Region-specific leptin resistance within the hypothalamus of diet-induced obese mice, Endocrinology. 145 (2004) 4880-9. 10.1210/en.2004-0726.
[78] P.M. Smith, P. Brzezinska, F. Hubert, A. Mimee, D.H. Maurice, A.V. Ferguson, Leptin influences the excitability of area postrema neurons, Am J Physiol Regul Integr Comp Physiol. 310 (2016) R440-8. 10.1152/ajpregu.00326.2015.
[79] C.G. Liberini, C.N. Boyle, C. Cifani, M. Venniro, B.T. Hope, T.A. Lutz, Amylin receptor components and the leptin receptor are co-expressed in single rat area postrema neurons, Eur J Neurosci. 43 (2016) 653-61. 10.1111/ejn.13163.
[80] L. Huo, L. Maeng, C. Bjorbaek, H.J. Grill, Leptin and the control of food intake: neurons in the nucleus of the solitary tract are activated by both gastric distension and leptin, Endocrinology. 148 (2007) 2189-97. 10.1210/en.2006-1572.
[81] S.R. Smith, L.J. Aronne, C.M. Burns, N.C. Kesty, A.E. Halseth, C. Weyer, Sustained weight loss following 12-month pramlintide treatment as an adjunct to lifestyle intervention in obesity, Diabetes Care. 31 (2008) 1816-23. 10.2337/dc08-0029.
[82] J.P.H. Wilding, R.L. Batterham, S. Calanna, M. Davies, L.F. Van Gaal, I. Lingvay, et al., Once-Weekly Semaglutide in Adults with Overweight or Obesity, N Engl J Med. 384 (2021) 989-1002. 10.1056/NEJMoa2032183.
[83] B.B. Lake, R. Ai, G.E. Kaeser, N.S. Salathia, Y.C. Yung, R. Liu, et al., Neuronal subtypes and diversity revealed by single-nucleus RNA sequencing of the human brain, Science. 352 (2016) 1586-90. 10.1126/science.aaf1204.
[84] B.B. Lake, S. Codeluppi, Y.C. Yung, D. Gao, J. Chun, P.V. Kharchenko, et al., A comparative strategy for single-nucleus and single-cell transcriptomes confirms accuracy in predicted cell-type expression from nuclear RNA, Sci Rep. 7 (2017) 6031. 10.1038/s41598-017-04426-w.
[85] T.E. Bakken, R.D. Hodge, J.A. Miller, Z. Yao, T.N. Nguyen, B. Aevermann, et al., Single-nucleus and single-cell transcriptomes compared in matched cortical cell types, PLoS One. 13 (2018) e0209648. 10.1371/journal.pone.0209648.
[86] N. Thrupp, C. Sala Frigerio, L. Wolfs, N.G. Skene, N. Fattorelli, S. Poovathingal, et al., Single-Nucleus RNA-Seq Is Not Suitable for Detection of Microglial Activation Genes in Humans, Cell Rep. 32 (2020) 108189. 10.1016/j.celrep.2020.108189.
[87] H. Thorvaldsdottir, J.T. Robinson, J.P. Mesirov, Integrative Genomics Viewer (IGV): high-performance genomics data visualization and exploration, Brief Bioinform. 14 (2013) 178-92. 10.1093/bib/bbs017.
[88] M.J. Park, K. Chung, Endogenous lectin (RL-29) expression of the autonomic preganglionic neurons in the rat spinal cord, The Anatomical Record. 254 (1999) 54-60. 10.1002/%28SICI%291097-0185%2819990101%29254%3A1%3C53%3A%3AAID-AR7%3E3.0.CO%3B2-H.
[89] C.O. Miranda, K. Hegedus, H. Wildner, H.U. Zeilhofer, M. Antal, Morphological and neurochemical characterization of glycinergic neurons in laminae I-IV of the mouse spinal dorsal horn, J Comp Neurol. 530 (2022) 607-26. 10.1002/cne.25232.

[90] F. Guo, Y. Wang, TCF7l2, a nuclear marker that labels premyelinating oligodendrocytes and promotes oligodendroglial lineage progression, Glia. 71 (2023) 143-54. 10.1002/glia.24249.

[91] E. Weihe, C. Depboylu, B. Schutz, M.K. Schafer, L.E. Eiden, Three types of tyrosine hydroxylase-positive CNS neurons distinguished by dopa decarboxylase and VMAT2 co-expression, Cell Mol Neurobiol. 26 (2006) 659-78. 10.1007/s10571-006-9053-9.

[92] J. Sun, Y. Song, Z. Chen, J. Qiu, S. Zhu, L. Wu, et al., Heterogeneity and Molecular Markers for CNS Glial Cells Revealed by Single-Cell Transcriptomics, Cell Mol Neurobiol. 42 (2022) 2629-42. 10.1007/s10571-021-01159-3.

[93] M. Dallaporta, M.S. Bonnet, K. Horner, J. Trouslard, A. Jean, J.D. Troadec, Glial cells of the nucleus tractus solitarius as partners of the dorsal hindbrain regulation of energy balance: a proposal for a working hypothesis, Brain Res. 1350 (2010) 35-42. 10.1016/j.brainres.2010.04.025.

[94] J. Kalucka, L. de Rooij, J. Goveia, K. Rohlenova, S.J. Dumas, E. Meta, et al., Single-Cell Transcriptome Atlas of Murine Endothelial Cells, Cell. 180 (2020) 764-79 e20. 10.1016/j.cell.2020.01.015.

[95] N. Dani, R.H. Herbst, C. McCabe, G.S. Green, K. Kaiser, J.P. Head, et al., A cellular and spatial map of the choroid plexus across brain ventricles and ages, Cell. 184 (2021) 3056-74 e21. 10.1016/j.cell.2021.04.003.

[96] B. Ray, J.A. Bailey, S. Sarkar, D.K. Lahiri, Molecular and immunocytochemical characterization of primary neuronal cultures from adult rat brain: Differential expression of neuronal and glial protein markers, J Neurosci Methods. 184 (2009) 294-302. 10.1016/j.jneumeth.2009.08.018.

[97] S.E. Lauri, M. Ryazantseva, E. Orav, A. Vesikansa, T. Taira, Kainate receptors in the developing neuronal networks, Neuropharmacology. 195 (2021) 108585. 10.1016/j.neuropharm.2021.108585.

[98] Y.H. Song, J. Yoon, S.H. Lee, The role of neuropeptide somatostatin in the brain and its application in treating neurological disorders, Exp Mol Med. 53 (2021) 328-38. 10.1038/s12276-021-00580-4.

[99] H.W. Song, K.L. Foreman, B.D. Gastfriend, J.S. Kuo, S.P. Palecek, E.V. Shusta, Transcriptomic comparison of human and mouse brain microvessels, Sci Rep. 10 (2020) 12358. 10.1038/s41598-020-69096-7.

[100] L. Xu, Y. Yao, Central Nervous System Fibroblast-Like Cells in Stroke and Other Neurological Disorders, Stroke. 52 (2021) 2456-64. 10.1161/STROKEAHA.120.033431.

[101] U. Ernsberger, H. Rohrer, Sympathetic tales: subdivisons of the autonomic nervous system and the impact of developmental studies, Neural Dev. 13 (2018) 20. 10.1186/s13064-018-0117-6.

[102] C.R. Gajera, H. Emich, O. Lioubinski, A. Christ, R. Beckervordersandforth-Bonk, K. Yoshikawa, et al., LRP2 in ependymal cells regulates BMP signaling in the adult neurogenic niche, J Cell Sci. 123 (2010) 1922-30. 10.1242/jcs.065912.

[103] A. MacDonald, B. Lu, M. Caron, N. Caporicci-Dinucci, D. Hatrock, K. Petrecca, et al., Single Cell Transcriptomics of Ependymal Cells Across Age, Region and Species Reveals Cilia-Related and Metal Ion Regulatory Roles as Major Conserved Ependymal Cell Functions, Front Cell Neurosci. 15 (2021) 703951. 10.3389/fncel.2021.703951.

[104] H.W. Jeong, R. Dieguez-Hurtado, H. Arf, J. Song, H. Park, K. Kruse, et al., Single-cell transcriptomics reveals functionally specialized vascular endothelium in brain, Elife. 11 (2022) 10.7554/eLife.57520.

[105] K. Huizer, D.A.M. Mustafa, J.C. Spelt, J.M. Kros, A. Sacchetti, Improving the characterization of endothelial progenitor cell subsets by an optimized FACS protocol, PLoS One. 12 (2017) e0184895. 10.1371/journal.pone.0184895.

[106] E. Gerrits, Y. Heng, E. Boddeke, B.J.L. Eggen, Transcriptional profiling of microglia; current state of the art and future perspectives, Glia. 68 (2020) 740-55. 10.1002/glia.23767.

[107] P.T. Shah, J.A. Stratton, M.G. Stykel, S. Abbasi, S. Sharma, K.A. Mayr, et al., Single-Cell Transcriptomics and Fate Mapping of Ependymal Cells Reveals an Absence of Neural Stem Cell Function, Cell. 173 (2018) 1045-57 e9. 10.1016/j.cell.2018.03.063.

[108] C.G. Causing, A. Gloster, R. Aloyz, S.X. Bamji, E. Chang, J. Fawcett, et al., Synaptic Innervation Density Is Regulated by Neuron-Derived BDNF, Neuron. 18 (1997) 257–67. https://www.cell.com/fulltext/S0896-6273(00)80266-4#secd33944447e474.

[109] Y. Zhang, S.A. Sloan, L.E. Clarke, C. Caneda, C.A. Plaza, P.D. Blumenthal, et al., Purification and Characterization of Progenitor and Mature Human Astrocytes Reveals Transcriptional and Functional Differences with Mouse, Neuron. 89 (2016) 37-53. 10.1016/j.neuron.2015.11.013.

[110] F. Langlet, Tanycyte Gene Expression Dynamics in the Regulation of Energy Homeostasis, Front Endocrinol (Lausanne). 10 (2019) 286. 10.3389/fendo.2019.00286.

[111] O. Uriarte Huarte, D. Kyriakis, T. Heurtaux, Y. Pires-Afonso, K. Grzyb, R. Halder, et al., Single-Cell Transcriptomics and In Situ Morphological Analyses Reveal Microglia Heterogeneity Across the Nigrostriatal Pathway, Front Immunol. 12 (2021) 639613. 10.3389/fimmu.2021.639613.

[112] R.E. Pepper, K.A. Pitman, C.L. Cullen, K.M. Young, How Do Cells of the Oligodendrocyte Lineage Affect Neuronal Circuits to Influence Motor Function, Memory and Mood?, Front Cell Neurosci. 12 (2018) 399. 10.3389/fncel.2018.00399.

[113] A. Maegawa, K. Murata, K. Kuroda, S. Fujieda, Y. Fukazawa, Cellular Profiles of Prodynorphin and Preproenkephalin mRNA-Expressing Neurons in the Anterior Olfactory Tubercle of Mice, Front Neural Circuits. 16 (2022) 908964. 10.3389/fncir.2022.908964.

[114] S.T. Hentges, V. Otero-Corchon, R.L. Pennock, C.M. King, M.J. Low, Proopiomelanocortin expression in both GABA and glutamate neurons, J Neurosci. 29 (2009) 13684-90. 10.1523/JNEUROSCI.3770-09.2009.

[115] W. Sun, A. Cornwell, J. Li, S. Peng, M.J. Osorio, N. Aalling, et al., SOX9 Is an Astrocyte-Specific Nuclear Marker in the Adult Brain Outside the Neurogenic Regions, J Neurosci. 37 (2017) 4493-507. 10.1523/JNEUROSCI.3199-16.2017.

[116] A.T. Lee, D. Vogt, J.L. Rubenstein, V.S. Sohal, A class of GABAergic neurons in the prefrontal cortex sends long-range projections to the nucleus accumbens and elicits acute avoidance behavior, J Neurosci. 34 (2014) 11519-25. 10.1523/JNEUROSCI.1157-14.2014.

[117] M. Vanlandewijck, L. He, M.A. Mae, J. Andrae, K. Ando, F. Del Gaudio, et al., A molecular atlas of cell types and zonation in the brain vasculature, Nature. 554 (2018) 475-80. 10.1038/nature25739.

[118] M. Carlen, K. Meletis, C. Goritz, V. Darsalia, E. Evergren, K. Tanigaki, et al., Forebrain ependymal cells are Notch-dependent and generate neuroblasts and astrocytes after stroke, Nat Neurosci. 12 (2009) 259-67. 10.1038/nn.2268.

[119] J. Garcia-Revilla, A. Boza-Serrano, A.M. Espinosa-Oliva, M.S. Soto, T. Deierborg, R. Ruiz, et al., Galectin-3, a rising star in modulating microglia activation under conditions of neurodegeneration, Cell Death Dis. 13 (2022) 628. 10.1038/s41419-022-05058-3.

[120] A.C. Yang, R.T. Vest, F. Kern, D.P. Lee, M. Agam, C.A. Maat, et al., A human brain vascular atlas reveals diverse mediators of Alzheimer's risk, Nature. 603 (2022) 885-92. 10.1038/s41586-021-04369-3.

[121] S. Chasseigneaux, Y. Moraca, V. Cochois-Guegan, A.C. Boulay, A. Gilbert, S. Le Crom, et al., Isolation and differential transcriptome of vascular smooth muscle cells and mid-capillary pericytes from the rat brain, Sci Rep. 8 (2018) 12272. 10.1038/s41598-018-30739-5.

[122] Z. Gao, K. Ure, J.L. Ables, D.C. Lagace, K.A. Nave, S. Goebbels, et al., Neurod1 is essential for the survival and maturation of adult-born neurons, Nat Neurosci. 12 (2009) 1090-2. 10.1038/nn.2385.

[123] T. Kodama, S. Guerrero, M. Shin, S. Moghadam, M. Faulstich, S. du Lac, Neuronal classification and marker gene identification via single-cell expression profiling of brainstem vestibular neurons subserving cerebellar learning, J Neurosci. 32 (2012) 7819-31. 10.1523/JNEUROSCI.0543-12.2012.

[124] J. Manjarrez-Marmolejo, J. Franco-Pérez, Gap Junction Blockers- An Overview of their Effects on Induced Seizures in Animal Models, Current Neuropharmacology. 14 (2016) 759-71. 10.2174/1570159X14666160603115.

[125] T. Paretkar, E. Dimitrov, Activation of enkephalinergic (Enk) interneurons in the central amygdala (CeA) buffers the behavioral effects of persistent pain, Neurobiol Dis. 124 (2019) 364-72. 10.1016/j.nbd.2018.12.005.

[126] Z. Zhang, Z. Ma, W. Zou, H. Guo, M. Liu, Y. Ma, et al., The Appropriate Marker for Astrocytes: Comparing the Distribution and Expression of Three Astrocytic Markers in Different Mouse Cerebral Regions, Biomed Res Int. 2019 (2019) 9605265. 10.1155/2019/9605265.

[127] A.M. Jurga, M. Paleczna, J. Kadluczka, K.Z. Kuter, Beyond the GFAP-Astrocyte Protein Markers in the Brain, Biomolecules. 11 (2021) 10.3390/biom11091361.

[128] V. Dyachuk, A. Furlan, M.K. Shahidi, M. Giovenco, N. Kaukua, C. Konstantinidou, et al., Parasympathetic neurons originate from nerve-associated peripheral glial progenitors, Science. 345 (2014) 82-7. 10.1126/science.1253281.

[129] M.S. Erwig, J. Patzig, A.M. Steyer, P. Dibaj, M. Heilmann, I. Heilmann, et al., Anillin facilitates septin assembly to prevent pathological outfoldings of central nervous system myelin, eLife. 8 (2019) 10.7554/eLife.43888.

[130] J. Spaas, W.M.A. Franssen, C. Keytsman, L. Blancquaert, T. Vanmierlo, J. Bogie, et al., Carnosine quenches the reactive carbonyl acrolein in the central nervous system and attenuates autoimmune neuroinflammation, J Neuroinflammation. 18 (2021) 255. 10.1186/s12974-021-02306-9.

[131] J. DeSisto, R. O'Rourke, H.E. Jones, B. Pawlikowski, A.D. Malek, S. Bonney, et al., Single-Cell Transcriptomic Analyses of the Developing Meninges Reveal Meningeal Fibroblast Diversity and Function, Dev Cell. 54 (2020) 43-59 e4. 10.1016/j.devcel.2020.06.009.

[132] D.S. Liu, T.L. Xu, Cell-Type Identification in the Autonomic Nervous System, Neurosci Bull. 35 (2019) 145-55. 10.1007/s12264-018-0284-9.

[133] B.J. Kang, D.A. Chang, D.D. Mackay, G.H. West, T.S. Moreira, A.C. Takakura, et al., Central nervous system distribution of the transcription factor Phox2b in the adult rat, J Comp Neurol. 503 (2007) 627-41. 10.1002/cne.21409.

[134] M. Adler, N. Moriel, A. Goeva, I. Avraham-Davidi, S. Mages, T.S. Adams, et al., Emergence of division of labor in tissues through cell interactions and spatial cues, Cell Rep. 42 (2023) 112412. 10.1016/j.celrep.2023.112412.

[135] A. Steimel, J. Suh, A. Hussainkhel, S. Deheshi, J.M. Grants, R. Zapf, et al., The C. elegans CDK8 Mediator module regulates axon guidance decisions in the ventral nerve cord and during dorsal axon navigation, Dev Biol. 377 (2013) 385-98. 10.1016/j.ydbio.2013.02.009.

[136] T. Daiber, C.J. VanderZwan-Butler, G.J. Bashaw, T.A. Evans, Conserved and divergent aspects of Robo receptor signaling and regulation between Drosophila Robo1 and C. elegans SAX-3, Genetics. 217 (2021) 10.1093/genetics/iyab018.

[137] S. Schmetsdorf, U. Gärtner, T. Arendt, Constitutive Expression of Functionally Active Cyclin-Dependent Kinases and Their Binding Partners Suggests Noncanonical Functions of Cell Cycle Regulators in Differentiated Neurons, Cerebral Cortex. 17 (2007) 1821–9. https://doi.org/10.1093/cercor/bhl091.

[138] K.K. Kummer, M. Zeidler, T. Kalpachidou, M. Kress, Role of IL-6 in the regulation of neuronal development, survival and function, Cytokine. 144 (2021) 155582. 10.1016/j.cyto.2021.155582.

[139] P. März, J.G. Cheng, R.A. Gadient, P.H. Patterson, T. Stoyan, U. Otten, et al., Sympathetic neurons can produce and respond to interleukin 6, Proc Natl Acad Sci. 95 (1998) 3251-6. 10.1073/pnas.95.6.3251.

[140] K.M. McGrail, J.M. Phillips, K.J. Sweadner, Immunofluorescent localization of three Na,K-ATPase isozymes in the rat central nervous system: both neurons and glia can express more than one Na,K-ATPase., J Neurosci. 11 (1991) 381-91. 10.1523/JNEUROSCI.11-02-00381.1991.

[141] H. Poulsen, H. Khandelia, J.P. Morth, M. Bublitz, O.G. Mouritsen, J. Egebjerg, et al., Neurological disease mutations compromise a C-terminal ion pathway in the Na(+)/K(+)-ATPase, Nature. 467 (2010) 99-102. 10.1038/nature09309.

[142] A. Abousaab, J. Warsi, B. Elvira, F. Lang, Caveolin-1 Sensitivity of Excitatory Amino Acid Transporters EAAT1, EAAT2, EAAT3, and EAAT4, J Membr Biol. 249 (2016) 239-49. 10.1007/s00232-015-9863-0.

[143] E.R. Bongarzone, C.W. Campagnoni, K. Kampf, E.C. Jacobs, V.W. Handley, V. Schonmann, et al., Identification of a new exon in the myelin proteolipid protein gene encoding novel protein isoforms that are restricted to the somata of oligodendrocytes and neurons., J Neurosci. 19 (1999) 8349-57. 10.1523/JNEUROSCI.19-19-08349.

[144] L.F. Nunnelly, M. Campbell, D.I. Lee, P. Dummer, G. Gu, V. Menon, et al., St18 specifies globus pallidus projection neuron identity in MGE lineage, Nat Commun. 13 (2022) 7735. 10.1038/s41467-022-35518-5.

[145] C. Plachez, C. Lindwall, N. Sunn, M. Piper, R.X. Moldrich, C.E. Campbell, et al., Nuclear factor I gene expression in the developing forebrain, J Comp Neurol. 508 (2008) 385-401. 10.1002/cne.21645.

[146] J. Fraser, A. Essebier, A.S. Brown, R.A. Davila, D. Harkins, O. Zalucki, et al., Common Regulatory Targets of NFIA, NFIX and NFIB during Postnatal Cerebellar Development, Cerebellum. 19 (2020) 89-101. 10.1007/s12311-019-01089-3.

[147] L. Dubois , A. Vincent, The COE--Collier/Olf1/EBF--transcription factors: structural conservation and diversity of developmental functions, 108. 3-12 (2001) 10.1016/s0925-4773(01)00486-5.

[148] Y. Liu, T. Lear, O. Iannone, S. Shiva, C. Corey, S. Rajbhandari, et al., The Proapoptotic F-box Protein Fbxl7 Regulates Mitochondrial Function by Mediating the Ubiquitylation and Proteasomal Degradation of Survivin, J Biol Chem. 290 (2015) 11843-52. 10.1074/jbc.M114.629931.

[149] H. Kim, N.C. Berens, N.E. Ochandarena, B.D. Philpot, Region and Cell Type Distribution of TCF4 in the Postnatal Mouse Brain, Front Neuroanat. 14 (2020) 42. 10.3389/fnana.2020.00042.

[150] A. Sirp, A. Shubina, J. Tuvikene, L. Tamberg, C.S. Kiir, L. Kranich, et al., Expression of alternative transcription factor 4 mRNAs and protein isoforms in the developing and adult rodent and human tissues, Front Mol Neurosci. 15 (2022) 1033224. 10.3389/fnmol.2022.1033224.

[151] R.D. Hodge, T.E. Bakken, J.A. Miller, K.A. Smith, E.R. Barkan, L.T. Graybuck, et al., Conserved cell types with divergent features in human versus mouse cortex, Nature. 573 (2019) 61-8. 10.1038/s41586-019-1506-7.

[152] T. Kuroda, S. Yasuda, S. Tachi, S. Matsuyama, S. Kusakawa, K. Tano, et al., SALL3 expression balance underlies lineage biases in human induced pluripotent stem cell differentiation, Nat Commun. 10 (2019) 2175. 10.1038/s41467-019-09511-4.

[153] F. Morello, D. Borshagovski, M. Survila, L. Tikker, S. Sadik-Ogli, A. Kirjavainen, et al., Molecular Fingerprint and Developmental Regulation of the Tegmental GABAergic and Glutamatergic Neurons Derived from the Anterior Hindbrain, Cell Rep. 33 (2020) 108268. 10.1016/j.celrep.2020.108268.

[154] L. Wolf, C.S. Gao, K. Gueta, Q. Xie, T. Chevallier, N.R. Podduturi, et al., Identification and characterization of FGF2-dependent mRNA: microRNA networks during lens fiber cell differentiation, G3 (Bethesda). 3 (2013) 2239-55. 10.1534/g3.113.008698.

[155] H. Liu, M. Aramaki, Y. Fu, D. Forrest, Retinoid-Related Orphan Receptor beta and Transcriptional Control of Neuronal Differentiation, Curr Top Dev Biol. 125 (2017) 227-55. 10.1016/bs.ctdb.2016.11.009.

[156] M.G. Del Barrio, S. Bourane, K. Grossmann, R. Schule, S. Britsch, D.D. O'Leary, et al., A transcription factor code defines nine sensory interneuron subtypes in the mechanosensory area of the spinal cord, PLoS One. 8 (2013) e77928. 10.1371/journal.pone.0077928.

[157] Y. Li, A. Osuma, E. Correa, M.A. Okebalama, P. Dao, O. Gaylord, et al., Establishment and maintenance of motor neuron identity via temporal modularity in terminal selector function, Elife. 9 (2020) 10.7554/eLife.59464.

[158] D. Moruzzo, L. Nobbio, B. Sterlini, G.G. Consalez, F. Benfenati, A. Schenone, et al., The Transcription Factors EBF1 and EBF2 Are Positive Regulators of Myelination in Schwann Cells, Mol Neurobiol. 54 (2017) 8117-27. 10.1007/s12035-016-0296-2.

[159] M.A. Jimenez, P. Akerblad, M. Sigvardsson, E.D. Rosen, Critical role for Ebf1 and Ebf2 in the adipogenic transcriptional cascade, Mol Cell Biol. 27 (2007) 743-57. 10.1128/MCB.01557-06.

[160] H. Yu, M. Rubinstein, M.J. Low, Developmental single-cell transcriptomics of hypothalamic POMC neurons reveal the genetic trajectories of multiple neuropeptidergic phenotypes, Elife. 11 (2022) 10.7554/eLife.72883.

[161] I. Singh, L. Wang, B. Xia, J. Liu, A. Tahiri, A. El Ouaamari, et al., Activation of arcuate nucleus glucagon-like peptide-1 receptor-expressing neurons suppresses food intake, Cell Biosci. 12 (2022) 178. 10.1186/s13578-022-00914-3.

[162] L. Xiao, D.P. Merullo, T.M.I. Koch, M. Cao, M. Co, A. Kulkarni, et al., Expression of FoxP2 in the basal ganglia regulates vocal motor sequences in the adult songbird, Nat Commun. 12 (2021) 2617. 10.1038/s41467-021-22918-2.

[163] T.T. Du, J.B. Dewey, E.L. Wagner, R. Cui, J. Heo, J.J. Park, et al., LMO7 deficiency reveals the significance of the cuticular plate for hearing function, Nat Commun. 10 (2019) 1117. 10.1038/s41467-019-09074-4.

[164] M.A. Wozniak, B.M. Baker, C.S. Chen, K.L. Wilson, The emerin-binding transcription factor Lmo7 is regulated by association with p130Cas at focal adhesions, PeerJ. 1 (2013) e134. 10.7717/peerj.134.

[165] T. Kawaue, A. Shitamukai, A. Nagasaka, Y. Tsunekawa, T. Shinoda, K. Saito, et al., Lzts1 controls both neuronal delamination and outer radial glial-like cell generation during mammalian cerebral development, Nat Commun. 10 (2019) 2780. 10.1038/s41467-019-10730-y.

[166] O. Randlett, L. Poggi, F.R. Zolessi, W.A. Harris, The oriented emergence of axons from retinal ganglion cells is directed by laminin contact in vivo, Neuron. 70 (2011) 266-80. 10.1016/j.neuron.2011.03.013.

[167] N. Ichikawa-Tomikawa, J. Ogawa, V. Douet, Z. Xu, Y. Kamikubo, T. Sakurai, et al., Laminin alpha1 is essential for mouse cerebellar development, Matrix Biol. 31 (2012) 17-28. 10.1016/j.matbio.2011.09.002.

[168] E.S. Liau, S. Jin, Y.C. Chen, W.S. Liu, M. Calon, S. Nedelec, et al., Single-cell transcriptomic analysis reveals diversity within mammalian spinal motor neurons, Nat Commun. 14 (2023) 46. 10.1038/s41467-022-35574-x.

1303 Figure legends

1304 Figure 1: Two layers of cell identity for the murine DVC cells from snRNA-seq data

1305 **A.** Adult C57BL/6J mice were subjected to 10X Genomics-based snRNA barcoding and
1306 sequencing after dissection of their DVC (n=30). **B.** Labeled UMAP plot of the mouse DVC
1307 (cells n=99,740) at the lowest resolution (layer 1) including 4 cell identities, and **C.** the cell
1308 class (layer 2) including 18. **D.** Heatmap of the main marker genes (average log2FC
1309 expression >80 percentiles of upregulated genes) for each neuronal class of the mouse DVC
1310 (MAST algorithm; neurons n= 48,131; adj. p<0.05). Each column is one cell and each row is
1311 one marker gene. **E.** Stacked barplot of log-normalized counts of genes for 10 transcripts (i.e.
1312 *Gad2*, *Gad1*, *Slc6a5*, *Slc17a6*, *Slc18a2*, *Addc*, *Sst*, *Npy*, *Cck* and *Slc5a7*) related to
1313 transmission/release of 8 neurotransmitters and neuropeptides, by neuronal cell class. Each
1314 bar represents one neuron (n=48,131).

1315 snRNA-seq=single-nuclei RNA-sequencing; DVC=dorsal vagal complex; FACs=fluorescence-activated cell
1316 sorting; UMAP=uniform manifold approximation and projection; FC=fold-change; adj.=adjusted;
1317 GABA=gamma-aminobutyric acid

1318

1319 Figure 2: Third layer of non-neuronal murine DVC cell identities

1320 **A.** Labeled UMAP plot of the mouse DVC with the 15 non-neuronal cell identities shown (total
1321 cells n=99,740; non-neuronal cells n=51,609). **B.** UMAP plot showing scaled expression of
1322 *Gfap*, *Gria2* and *Kcnj3* genes in Ca^+-permeable astrocytes (circled; total cells n=99,740; Ca^+-
1323 permeable astrocytes n=1,719). **C.** Barplot of log-normalized expression of six genes in
1324 oligodendrocytes (premyelinating n=267; myelinating intermediate n=25,692; myelinating n=
1325 6,170). Only premyelinating oligodendrocytes lack expression of *Mobp*, involved in myelin
1326 formation. Reduction of *Synpr* and *Opalin* expression is observed as *Anln* and *Aff3* increase
1327 in myelinating oligodendrocytes. **D.** Balloon plot of the main cell types of non-neuronal cells
1328 and neurons showing average log-normalized counts of their marker genes (MAST algorithm;
1329 adj. p<0.05). Markers shown are upregulated genes in >80% of cells per group with average
1330 log2FC>4, or upregulated in >70% of cells with average log2FC>8.

1331 DVC=dorsal vagal complex; UMAP=uniform manifold approximation and projection; APNTS=Area postrema
1332 and nucleus of the solitary tract; OL=oligodendrocyte; OPC=oligodendrocyte precursor cell; Smc=smooth
1333 muscle cells

1334

1335 Figure 3: Neuronal populations of the murine DVC

1336 **A.** Labeled UMAP plot with the neuronal layer 3 cell identities (neurons n=48,131). **B.**
1337 Monoamine class balloon plot showing average log-normalized expression of marker genes
1338 for each cell identity (MAST algorithm; M0 cells n=770, M1 cells n=551, M2 cells n=666 and
1339 M3 cells n=2,593; adj. p<0.05), and **C.** heatmap of expression of monoamine related genes.
1340 In the heatmap, each column represents one cell and each row, one gene. **D.** Barplot of *Gcg*

1341 average log-normalized expression by neuronal cell identity. **E.** UMAP plot showing the
1342 expression of leptin receptor and prolactin receptor genes in neurons. The GLP1 cluster is
1343 highlighted (GLP1 cells n=153). **F.** Stacked barplot of the proportion of cells expressing one
1344 or more GABA-related genes (i.e. *Slc32a1*, *Gad1*, *Gad2*) and glutamate-related genes (i.e.
1345 *Slc17a6*, *Slc17a7*). The proportion of cells per cell group co-expressing GABA and glutamate
1346 associated genes are shown in purple. Only cells with log-normalized counts >0 were
1347 considered to express the genes.
1348 DVC=dorsal vagal complex; UMAP=uniform manifold approximation and projection; Res.=resolution;
1349 GABA=gamma-aminobutyric acid
1350

1351 Figure 4: *Th* and *Cck* co-expression in the DVC

1352 **A.** UMAP plot of neuronal *Th* and *Cck* scaled expression and cells with co-expression of both
1353 genes (neurons n=48,131; *Th*-expressing neurons n=764; *Cck*-expressing neurons n=3,821;
1354 *Th*|*Cck* co-expressing neurons n=80). On the right plot, cells highlighted in magenta are the
1355 co-expressing neurons. The three neuronal cell identities in which the majority of nuclear co-
1356 expression of *Th* and *Cck* mRNA is found, as well as the percentage of total co-expressing
1357 neurons, are shown. **B.** *In-situ* hybridization of *Cck* and *Th* mRNA in coronal mouse DVC
1358 sections corresponding to -7.2mm and -7.56mm relative to bregma showing overlap of
1359 *Th*|*Cck*. Some of the cells with overlapping signal are highlighted with an arrow in the
1360 enhanced merged image.
1361 DVC=dorsal vagal complex; UMAP=uniform manifold approximation and projection
1362

1363 Figure 5: The murine DVC cell hierarchy

1364 **A.** Dendrogram of the harmonized hierarchy which incorporates cells from Ludwig and our
1365 datasets. Orange cell identities are a fourth layer of cell identity resolution obtained as some
1366 of the Ludwig dataset identities are subgroups of our original cell identities at their highest
1367 resolution. Magenta labels represent layer 3 of cellular granularity. These two layers are
1368 considered high-resolution. **B.** UMAP plot of the integration between our and Ludwig datasets
1369 using treeArches (cells n=171,868). **C.** Pairwise heatmap showing the proportion of cells
1370 originally labeled in this study and in Ludwig dataset (y-axis), predicted to belong to each
1371 identity group (x-axis) by treeArches using our learned harmonized hierarchy. In blue are the
1372 labels considered non-specific for a high-resolution cell identity (n=2,324; 1.3%). In pink are
1373 the cell labels for rejected cells, therefore not assigned any identity by treeArches (n=3,108;
1374 1.8%). **D.** UMAP plot of the Dowsett dataset labeled through treeArches using the learned
1375 harmonized hierarchy representation from our murine DVC atlas. The 'unlabeled' cells include
1376 those rejected by the algorithm and thus without an assigned identity, and those with an

1377 unspecific layer-3/4 label. For example, some were labeled 'neuron' or 'monoamine-class'
1378 but without a high-resolution cell identity.
1379 UMAP=uniform manifold approximation and projection; APNTS=Area postrema and nucleus of the solitary tract;
1380 Lnc=long non-coding; OL=oligodendrocyte; OPC=oligodendrocyte precursor cell; Neur=neuronal;
1381 COE=collier/Olf1/EBF transcription factor
1382

1383 Figure 6: The snRNA-seq derived cell identities for the rat DVC

1384 **A.** Schematic of the pipeline for snRNA-seq of the rat DVC. **B.** Labeled UMAP plots of the low
1385 resolution (i.e. layers 1 and 2 of granularity) and **C.** high resolution (i.e. layer 3) cell identities
1386 in our rat DVC dataset (cells n=12,167). We labeled four layer-1, nineteen layer-2 and fifty-
1387 two layer-3 cell identities. Those labels novel to this dataset and not present in the murine
1388 data are highlighted with a pink ♦ symbol. We found a small cluster (cells n=35) that we could
1389 not corroborate its identity at any layer of cellular granularity that we named 'unspecific'.
1390 snRNA-seq=single-nuclei RNA-sequencing; DVC=dorsal vagal complex; FACs=fluorescence-activated cell
1391 sorting; UMAP=uniform manifold approximation and projection; APNTS=Area postrema and nucleus of the
1392 solitary tract; Lnc=long non-coding; OL=oligodendrocyte; OPC=cursor cell; Neur=neuronal;
1393 COE=collier/Olf1/EBF transcription factors
1394

1395 Figure 7: Two novel neuronal classes specific to the rat DVC

1396 **A.** Balloon plots comparing the expression of the marker genes of the two novel neuronal
1397 classes found in rats (cells n=12,167): immunity-akin and the ortus-akin classes (framed in
1398 gray). Expression is shown across the layer-2 rat cell identities. Based on the expression of
1399 two DVC neuronal markers *Mtus2* and *Syt1*, we corroborated those cell classes contain
1400 neurons, and not microglial or vascular/endothelial cells (In orange and red, respectively).
1401 The immunity-akin class (n=48 neurons) shares high expression of *Cst3*, *Inpp5d*, *Csf1r*,
1402 *Slco2b1* and *Lyn* with microglial cells. Meanwhile, the ortus-akin class (n=34 neurons) shows
1403 higher overlap of gene expression markers (i.e. *Arhgap31*, *Pdgfra*, *Bcas1*, *Ppfibp1* and *Itga9*)
1404 with OPCs (highlighted with a ♦ symbol). Mouse cell identities (cells n=99,740) do not show
1405 these expression patterns (framed in black). Average expression was calculated using log-
1406 normalized counts. **B.** Violin plots of scaled expression of 10 genes (i.e. *Glp1r, Gfral, Calcr,*
1407 *Ramp3, Gipr, Lepr, Cckar, Cckbr ,Mc4r* and *Prlr*) coding for metabolism-associated
1408 receptors in the Pdgfra and immunity-related rat neurons (Pdgfra neurons n=34; immunity-
1409 related neurons n=48). Pdgfra neurons are the only layer-3 identity within the ortus-akin class.
1410 An overlapping dotplot shows one dot per cell. **C.** Immunofluorescent detection of PDGFRA
1411 in mouse and rat DVC. Pink arrowheads point to cells with OPC morphology, white
1412 arrowheads point to cells with fibroblast morphology and the yellow arrowhead points to cells
1413 with neural morphology. **D.** Co-staining for PDGFRA and HuC/D in rat DVC with high

magnification (right images) of area postrema PDGFRA-expressing cells . Yellow arrowheads indicate colocalization of HuC/D and PDGFRA.

DVC=dorsal vagal complex; OPC=oligodendrocyte precursor cell; AP=area postrema; NTS=nucleus of the solitary tract; PDGFRA= Platelet-derived growth factor receptor A; CC=central canal

Figure 8: The rodent DVC cell hierarchy

A. UMAP plot of the integration between the murine hierarchy and our rat dataset using treeArches (cells n=184,035). **B.** Dendrogram of the harmonized hierarchy of our labeled rat dataset and the murine DVC hierarchy. We highlight the incorporated rat cell identities (blue and magenta). Those in magenta are the novel rat identities established by us. The immunity-akin and the ortus-akin classes were not found in the murine datasets. The M3 and M5 rat identities are subgroups of a Ludwig layer 4 cell identity, therefore yields a fifth layer within the monoamine neuronal class.

UMAP=uniform manifold approximation and projection; DVC=dorsal vagal complex; APNTS=Area postrema and nucleus of the solitary tract; Lnc=long non-coding; OL=oligodendrocyte; OPC=oligodendrocyte precursor cell; Neur=neuronal; COE=collier/Olf1/EBF transcription factors

Figure 9: Meal-related transcriptional changes in the mouse DVC

A. Horizontal barplots of the number of differential genes between refed and ad libitum fed, and refed and fasted mice in glial cells and neurons per layer-2 cell identity (MAST algorithm on log-normalized counts; adj. $p<0.05$; refed neurons n=14,396; refed glial cells n=18,019; ad libitum fed neurons n= 9,885; ad libitum fed glial cells n=4,610; fasted neurons n=8,829; fasted glial cells n=12,496). **B.** Venn Diagrams of the differentially expressed genes in magnaclass 1 and magnaclass 2 neurons between refed and ad libitum fed, and between refed and fasted treatments (MAST algorithm on log-normalized counts). The number of overlapping log2FC≥1 upregulated genes between the two magnaclasses per treatment are highlighted. The treatment-induced changes in only one cell class are shown as non-overlapping. The percentage is based on the total differential genes surveyed per comparison. **C.** Volcano plots of the differential genes in neurons belonging to the magnaclass 1 and the magnaclass 2 between refed and ad libitum fed, and **D.** refed and fasted treatments (MAST algorithm on log-normalized counts; adj. $p<0.05$). Each point represents one gene. Only genes upregulated or downregulated with a log2FC≥2 are labeled. Since we considered a minimum log fold-change of 0.1 between treatments per cell group, those genes with very low variance (i.e. log fold-change<0.1) were excluded from the differential expression analysis, therefore a variable number of genes are shown per comparison per identity, in the volcano plots.

DVC=dorsal vagal complex; vr=versus; OPC=oligodendrocyte precursor cell; FC=fold-change; adj.=adjusted; NS=non-significant

Supplementary Material

Figure S1: DVC-centric dissection protocol

A. Following euthanasia, the brain is removed from the mouse and briefly rinsed with PBS. To better visualize the brainstem, the cerebellum is removed with fine forceps. The brain is then placed within a mouse brain matrix with 1mm spacing between razor guides. In this example blades will be placed in the 12th (cut 1) and 14th (cut 2) razor guide (these sites are shown). Using fresh razors make two clean cuts in a single, smooth motion. The bottom showns the reference images of the mouse brain (from the Allen Brain Institute reference 3D mouse atlas) visualizing the location of brainstem and the AP/NTS. In these reference images, the cerebellum is not visualized. **B.** Resultant brainstem tissue from the first two cuts is then further cut twice more (cuts 3 &4) to keep the middle of the tissue where the DVC is located. This tissue is cut once more (cut 5) to generate a DVC-centric dissection. Reference images of the mouse brain (Coronal sections from the Allen Brain Institute reference atlas) displaying the rostral and caudal sides of tissue collected from cuts 1&2 and the location of cuts 3-5, are shown.

Figure S2: Mapping of *Gad2* and VGLUT2 in neurons

UMAP plot of the murine neurons (n=48,131) showing scaled log-normalized expression of **A.** *Gad2*, a gene related to GABA synthesis and transmission, **B.** and VGLUT2, a glutamate transporter. Cells with higher expression of *Gad2* belong to the neuronal magnaclass1, while cells with higher expression of VGLUT2 (*Slc17a6*) to the magnaclass2 (both highlighted in yellow in adjacent plots). However, the expression is not mutually exclusive among both classes, nor every neuron belonging to each class express the respective transcript.

UMAP=uniform manifold approximation and projection; GABA=gamma-aminobutyric acid; VGLUT2=vesicular glutamate transporter-2

Figure S3: Anatomical mapping of the DVC mouse layer-3 identities

Schematic diagram of the spatial localization for the 35 neuronal identities at layer 3 of resolution in the mouse DVC. Coronal sections from the mouse brain in the Allen Brain Atlas were used to manually map the top marker genes of each (MAST algorithm on log-normalized counts; adj. $p<0.05$) to the DVC.

AP=Area Postrema; NTS= Nucleus of the solitary trac; DMV= Dorsal motor nucleus of the vagus; CC= central canal; 12N= hypoglossal nucleus; Cu=Cuneate nucleus.

Figure S4: Mapping of DVC populations in a murine hypothalamic dataset

UMAP plots of a randomly selected subset of the HypoMap database (cells n=76,260; samples n=32) labeled **A.** by sample and **B.** by original curated cell class. **C.** Balloon plot

showing average expression of the top 5 upregulated gene markers of each neuronal DVC class (MAST algorithm; adj. $p<0.05$) in the neurons of the HypoMap subset (n=45,679). We selected the neuronal curated class cells from our initial HypoMap subset and reprocessed them, including clustering through *k*-nearest neighbors algorithm using the first 30 PCs and Harmony reduction embeddings. Resulting clusters at resolution 0.5 are shown. Average expression in the HypoMap neurons was calculated using log-normalized counts. **D.** Set of UMAP plots showing scaled expression of three genes (i.e. *Gfap*, *Gria2* and *Kcnj3*) which have a specific pattern of expression in murine DVC Ca^+-permeable astrocytes. The astrocytic population is circled in purple (astrocytes n=7,629) and while *Gfap* and *Gria2* expression is in agreement to what we observe in Ca^+-permeable astrocytes, in the hypothalamic astrocytes *Kcnj3* is not expressed. **E.** Set of UMAP plots of expression of *Aldh1a1* and *Stk39* which are markers of p-fibroblasts and s-fibroblasts in the DVC. The hypothalamic fibroblasts are circled in magenta (fibroblasts n=300).

DVC=dorsal vagal complex; UMAP=uniform manifold approximation and projection; AMPAr=α-amino-3-hydroxy-5-methyl-4-isoxazolepropionic acid receptor; GIRK1=G protein-coupled inwardly rectifying potassium channel 1; OPC=Oligodendrocyte precursor cell; NG=*Ng2* glial cell

<u>Figure S5: Mapping of DVC Ca^+-permeable astrocytes in other murine brain sites</u>

UMAP plots of a cortical/hippocampal astrocytes dataset by **A.** sample, **B.** brain area and **C.** original astrocyte type (cell n=1,811). Set of UMAP plots showing scaled expression of three genes (i.e. *Gfap, Gria2* and *Kcnj3*) which have a specific pattern of expression in murine DVC Ca^+-permeable astrocytes in **D.** cortical/hippocampal, **E.** forebrain, **F.** pons and **G.** spinal cord astrocytes. There is some overlap in *Gfap* and *Gria2* expression in cortex, hippocampus and forebrain, with almost no expression of *Kcnj3*. This is different from what we observe in DVC Ca^+-permeable astrocytes. In pons and the spinal cord, there is some expression of *Kcnj3*, but the *Gfap* and *Kcnj3* co-expression is rare.

<u>Figure S6: Trajectory inference of the oligodendrocyte lineage</u>

Dotplot of the two principal components obtained through dimensionality reduction using the main 50 principal components analysis on log-normalized gene expression data in oligodendrocytes (cells n=32,129) **A.** merged and **B.** by sample, and on Harmony embeddings in oligodendrocytes **C.** merged and **D.** by sample. Cellular trajectory was inferred using SCORPIUS also on normalized gene expression data (**A.** and **B.**) and on the Harmony embeddings (**C.** and **D.**), and drawn across the data points (black line). Each data point represents one cell.

OL=oligodendrocyte

1526 Figure S7: Murine DVC clusters

1527 **A.** UMAP plot of the mouse DVC clusters at resolution 1 (cells n=99,740). Cells from mice
1528 exposed to 5 food and aversion-related treatments were integrated using the Harmony
1529 algorithm in R and the resulting embeddings were used to calculate the clusters and UMAP
1530 projections. We subset and re-clustered three clusters containing oligodendrocytes, vascular
1531 cells and fibroblasts, respectively (highlighted). **B.** Violin plots of the two types of fibroblasts
1532 in cluster 26, distinguished by *Skt39* (stress-response 's-fibroblasts') and *Aldh1a1*
1533 (perivascular 'p-fibroblasts') expression. Each data point represents one cell (s-fibroblasts
1534 n=244; p-fibroblasts n=559). **C.** UMAP plot of subclusters from clusters 23
1535 (oligodendrocytes) and **D.** 27 (vascular cells) using the Harmony embeddings. Gene
1536 expression markers for cell populations were mapped (**Table S5**) and the smallest resolution
1537 that allowed to separate them was further used to label the cells. Cells in subclusters 1 and
1538 2 from cluster 23 were labeled 'premyelinating_OL' whilst subclusters 0 and 3 were labeled
1539 'myelinating_intermediate_OL'. In cluster 27, subcluster 7 was labeled 'pericyte', subcluster
1540 4 was labeled 'smooth_muscle' and the rest of the clusters were considered to be endothelial
1541 cells.

1542 DVC=dorsal vagal complex; Res.=resolution; UMAP=uniform manifold approximation and projection;
1543 OL=oligodendrocyte; smc=smooth muscle cell.

1544

1545 Figure S8: Mouse microglial activation states

1546 **A.** UMAP plot showing the mapping in the mouse DVC microglia (n=2,787).of monocyte
1547 (*Emilin2* and *Gda*) and microglial (*P2ry12* and *Fcrls*) known differential markers,
1548 corroborating the absence of monocytes in our dataset. **B.** UMAP plot of the microglia from
1549 the mouse DVC showing scaled log-normalized expression of *Cd5*, *Zbp1*, *Cxcl9* and *Cxcl10*.
1550 Microglia was subset and re-processed using the harmony integration embeddings to obtain
1551 the UMAP coordinates. **C.** Sub-clusters at resolution 0.2 of these microglial cells was
1552 performed and the **D.** top marker genes are shown in a balloon plot with average log-
1553 normalized counts (MAST algorithm; adj. $p<0.05$) along with astrocytes and
1554 oligodendrocytes (microglia n=2,787, oligodendrocytes n= 32,129, astrocytes n=11,693).
1555 Cluster C3 shares high expression of markers with oligodendrocytes (in purple) while cluster
1556 C5 shares markers with astrocytes (in red). Microglial markers are highlighted in orange.

1557 UMAP=uniform manifold approximation and projection; DVC=dorsal vagal complex

1558

1559 Figure S9: Mixed neurons sub-clustering

1560 UMAP plots with the mixed neurons of the mouse DVC (mixed neurons n=15,190) showing
1561 their **A.** original layer-3 identity and **B.** final sub-cluster. **C.** Heatmap of the top 5 marker genes
1562 (MAST algorithm; adj. $p<0.05$) expression for each sub-cluster in all neurons (i.e. mixed

1563 neurons and all other neuronal identities, neurons n= 48,131). Each column is one cell and
1564 each row is one marker gene. Some marker genes were duplicated for more than one sub-
1565 cluster (e.g. *Nrxn3* is marker of sub-clusters 2, 3, 8 and 10; *Pcdh9* is marker of sub-clusters
1566 6 and 8) therefore these genes are only shown once in the plot and highlighted in red.
1567 UMAP=uniform manifold approximation and projection; DVC=dorsal vagal complex
1568

1569 Figure S10: Initial murine cell hierarchy using our samples
1570 **A.** UMAP plot of the integration of our samples (based on the five mouse treatments
1571 administered to mice prior to euthanasia; see **Methods**) using treeArches. There were two
1572 cohorts of refed mice. **B.** UMAP plot of the fifty layer-3 cell identities obtained using the
1573 treeArches pipeline. **C.** Dendrogram showing the initial hierarchy of the three layers of cell
1574 identity established by us in this study.
1575 UMAP=uniform manifold approximation and projection; inj.=injected; APNTS=Area postrema and nucleus of
1576 the solitary tract; Lnc=long non-coding; OL=oligodendrocyte; OPC=oligodendrocyte precursor cell;
1577 COE=collier/Olf1/EBF transcription factors
1578

1579 Figure S11: Incorporation of the Ludwig dataset to our initial hierarchy using treeArches
1580 **A.** Barplot of log-normalized expression of OPC markers (i.e. *Pdgfra*, *Cspg4*, *C1ql1*) and
1581 premyelinating OL markers (i.e. *Bmp4*, *Fyn*) in the OPCs-labeled cells from the Ludwig
1582 dataset (total cells n=1,770; cells expressing >1 marker gene n=1,104). Cells labeled as
1583 OPCs in the Ludwig dataset are a mix of OPC and premyelinating OL. Some cells lack
1584 expression of the five marker genes used in this plot, they are represented on the left side
1585 with an empty bar and those expressing *Fyn*/*Bmp4* but not expressing the OPC markers are
1586 likely premyelinating OLs. Cells were ordered using hierarchical clustering based on these
1587 five gene expression data through the Ward's method in R. We only indicate the 'likely cell
1588 identity' for cells with expression of the five marker genes. **B.** UMAP showing the manual
1589 mapping of Ludwig and Dowsett neuronal clusters and identities in neurons from this study.
1590 We used the gene expression markers for all clusters from Ludwig and Dowsett to identify
1591 which of our neurons shared identity with those described in both publications. Only groups
1592 and clusters successfully mapped manually are shown. The Ludwig identities are in black,
1593 Dowsett identities are in blue and our identities are in purple. Most of neuronal clusters in
1594 both publicly available datasets, are subgroups of our cell identities.
1595 OPC=oligodendrocyte precursor cell; OL=oligodendrocyte; UMAP=uniform manifold approximation and
1596 projection; APNTS=Area postrema and nucleus of the solitary tract; Lnc=long non-coding;
1597 COE=collier/Olf1/EBF transcription factors
1598

1599 Figure S12: Rat DVC neurons

1600 **A.** Labeled UMAP plot with the neuronal layer 3 cell identities in our rat dataset (neurons
1601 n=4,721). Neurons were subset and re-processed to obtain the UMAP coordinates. **B.** Violin
1602 plots of scaled expression of 12 genes (i.e. *Gad2, Gad1, Slc6a5, Slc17a7, Slc17a6, Th, Ddc,*
1603 *Nos1, Sst, Npy, Cck* and *Slc5a7*) related to transmission/release of GABA, glutamate,
1604 monoamines, nitric oxide, somatostatin, neuropeptide-Y, cholecystokinin and acetylcholine
1605 in the Pdgfra and immunity-related rat neurons (Pdgfra neurons n=34; immunity-related
1606 neurons n=48). An overlapping dotplot shows one data point representing each cell.
1607 DVC=dorsal vagal complex; UMAP=uniform manifold approximation and projection; COE=collier/Olf1/EBF
1608 transcription factors; Lnc=long non-coding; GABA=gamma-aminobutyric acid
1609

1610 Figure S13: Dendrogram after incorporation of the rat dataset to the murine hierarchy

1611 Dendrogram (i.e. tree) resulting from incorporating our rat dataset (cells n=12,167) to the
1612 existing murine DVC cell hierarchy using treeArches. The rat cell populations in red that did
1613 not show similarity with the previously existing murine identities are appended at the bottom
1614 by treeArches (shown in red).
1615

1616 Figure S14: Expression of *Agrp* and *Hcrt* in DVC neurons

1617 **A.** UMAP plots of the neurons (n=48,131) from our murine DVC dataset showing scaled
1618 expression of *Agrp* and *Hcrt*. **B.** *In-situ* hybridization images of *Agrp* and *Hcrt* in the DVC
1619 show no exonic mRNA. We included tissue sections of the arcuate nucleus of the
1620 hypothalamus and in the lateral hypothalamus as controls, and *Agrp* and *Hcrt* were present
1621 in these sites, respectively. For each reaction, tissue from the same mouse was used through
1622 two different sections, one including the DVC and one including the hypothalamic region. **C.**
1623 UMAP plots of the Dowsett (n=8,288) and the Ludwig datasets neurons (n=49,392) showing
1624 scaled expression of *Agrp* and *Hcrt*. **D.** Genome visualization of reads coverage in the *Agrp*
1625 and *Hcrt* regions of the *Mus musculus* refdata-gex-mm10-2020-A reference from two of our
1626 mouse sample sequencing replicates. Resulting BAM files from the original murine DVC
1627 FASTQ files were obtained after processing. We visualized the reads from these BAM files
1628 that mapped to the *Agrp* and *Hcrt* genes using IGV v2.16.1[87]. The coverage of these genes
1629 (*Agrp* region: chr8:105,566,180–105,582,268; *Hcrt* region: chr11:100,761,693–100,762,931)
1630 are shown in gray. The majority of the reads mapped to the intronic regions of *Agrp*, and to
1631 the last part of the 3'-end of exon 2 and the 3'-untranslated region of *Hcrt*. **E.** UMAP plot of
1632 rat DVC neurons (n=4,721) showing scaled expression of *Agrp* and *Hcrt*. For all UMAP
1633 projections, neurons from each dataset were subset based on our labeling for our murine
1634 and rat datasets, the treeArches resulting labeling for the Dowsett dataset, and the original

1635 labeling from Ludwig and collaborators. Then the neurons were processed using Seurat[23]
1636 and integrated using Harmony[25], to yield the final UMAP embeddings.
1637 DVC=dorsal vagal complex; UMAP=uniform manifold approximation and projection; AP=area postrema;
1638 NTS=nucleus of the solitary tract; ARH=arcuate nucleus of the hypothalamus; 3v=third ventricle; ME=median
1639 eminence; LH=lateral hypothalamus. BAM=binary alignment map
1640

1641 Figure S15: Expression of metabolism-associated receptors in the DVC magnaclasses
1642 Violin plots of scaled expression of 10 genes (i.e. *Glp1r, Gfral, Calcr, Ramp3, Gipr, Lepr,*
1643 *Cckar, Cckbr ,Mc4r* and *Prlr*) coding for metabolism-associated receptors in the
1644 magnaclass1 and magnaclass2 neurons of the mouse DVC in fasted (magnaclass1 n=2,756;
1645 magnaclass2 n=2,789) and refed (magnaclass1 n=4,586; magnaclass2 n=4,423).
1646 DVC=dorsal vagal complex
1647

1648 Table S1: Filtering of our and Dowsett datasets during processing
1649 Compilation of statistics and cells processed for the initial high quality cell filtering per
1650 sample.
1651

1652 Table S2: Cluster filtering of our and Dowsett datasets during processing
1653 Compilation of low quality cluster analysis statistics to filter high quality clusters per sample.
1654

1655 Table S3: Singlets retained per dataset after processing
1656 Number of doublets and singlets identified by DoubletFinder[24] after initial filtering of our
1657 and Dowset dataset per sample. Doublets were removed from the datasets before sample
1658 integration with Harmony[25] (this step was not performed in the rat dataset as it was only
1659 one sample, n=2 rat DVC).
1660

1661 Table S4: Murine brain databases used to map our unlabeled mouse dataset
1662 We used four databases included in the scRNAseq v2.16.0[26-28, 31, 55] R package and
1663 the celldex v1.12.0 built-in mouse RNA-seq reference (which we called 'SingleR' database)
1664 using SingleR [30] function to transfer labels to our dataset in R[22]. The name, brain area
1665 and reference in which each database was made public are specified.
1666

1667 Table S5: Literature-derived markers per central nervous system cell identity
1668 We thoroughly searched in the literature for established markers at the mRNA and/or protein
1669 level. Some markers were found to be described for more than one cell population which are
1670 specified in columns 'notes' and 'notes_2'. After initial labeling of our murine dataset with the
1671 databases as described, we proceeded to obtain the average expression (on log-normalized

counts) of each gene coding for the markers for the labeled cells (i.e. astrocyte, endothelial, microglia, neuron and oligodendrocyte) and unlabeled cells (i.e. unknown). We also calculated the average expression for each cluster in our dataset, established during our processing pipeline, at resolution 1.0.

Table S6: Description of our DVC layer-3 neuronal cell identities established in mice

Neurons were subset and reprocessed before labeling at layer-3 granularity. The MAST algorithm[32] was used through Seurat v5[23]on scaled data with a log fold-change threshold of 0.25 and detection threshold on ≥40% of cells on each neuronal cluster at resolution 1.0. We searched the resulting gene expression markers in the literature and compiled them. We then based the names for our cell identities on these genes.

Table S7: Literature-derived markers per central nervous system cell identity

Breakdown of the cell identities (except neurons at layer 3 of cellular resolution) we established and corroborating using a combination of markers surveyed in **Table S2** and additional markers established using the FindConservedMarkers function from Seurat v5[23] package, indicating a cell state derived from the literature. For example, 's_fibroblasts' were named after finding high expression of *Stk39*, a stress-related marker[56].

Table S8: Expression of the murine DVC identity markers by rat DVC clusters

Average log-normalized expression of the top 5 gene expression markers of each of our murine layer-3 cell identities (except duplicated genes n=37, and mouse specific genes n=27; total genes included=186) by rat DVC cluster at resolution 2.0.

Table S9: Description of our DVC layer-3 neuronal cell identities established in rats

Rat neurons were subset and reprocessed before labeling at layers 2 and 3 of granularity. We used neuronal class gene expression markers to identify clusters at resolution 2.0 that belonged to each neuronal cell class. These cell classes were further subclustered and markers from Table S6 and UMAP projections were used to label each population in the dataset.

Table S10: Labeled cells in our murine dataset

Number of cell per treatment per identity layer 2.

1706 Table S11: Expression of neurotransmitter-related genes in our murine neurons
1707 Expression of genes coding for neurotransmitter synthesis enzymes TH, DBH, TPH, GABA,
1708 NOS, prohormone SST and primary neurotransmitter transporters VMAT2, VGLUT1, VGLUT2,
1709 GLYT2 per neuron in our dataset. Expression and glutamate and GABA release are specified
1710 as binary variables (i.e. 0=no expression; 1=expression) in the green and blue columns,
1711 respectively. The percentile of the log-normalized expression is shown. ~55% of the neurons
1712 display expression of genes related to the synthesis/release of >1 primary neurotransmitter.
1713
1714 Table S12: Receptor expression in magnaclasses 1 and 2 between meal-related treatments
1715 in mice
1716 Differential expression analysis (MAST algorithm)[32] results for genes coding for metabolism
1717 related receptors between meal-related treatments (i.e. refed versus ad libitum fed, and refed
1718 versus overnight fasted) and per neuronal magnaclass. If a receptor is missing for any given
1719 comparison for any of the magnaclasses, the log fold-change of that gene between both
1720 treatments in that neuronal class was <0.1, therefore it is not reported (see **Methods**).

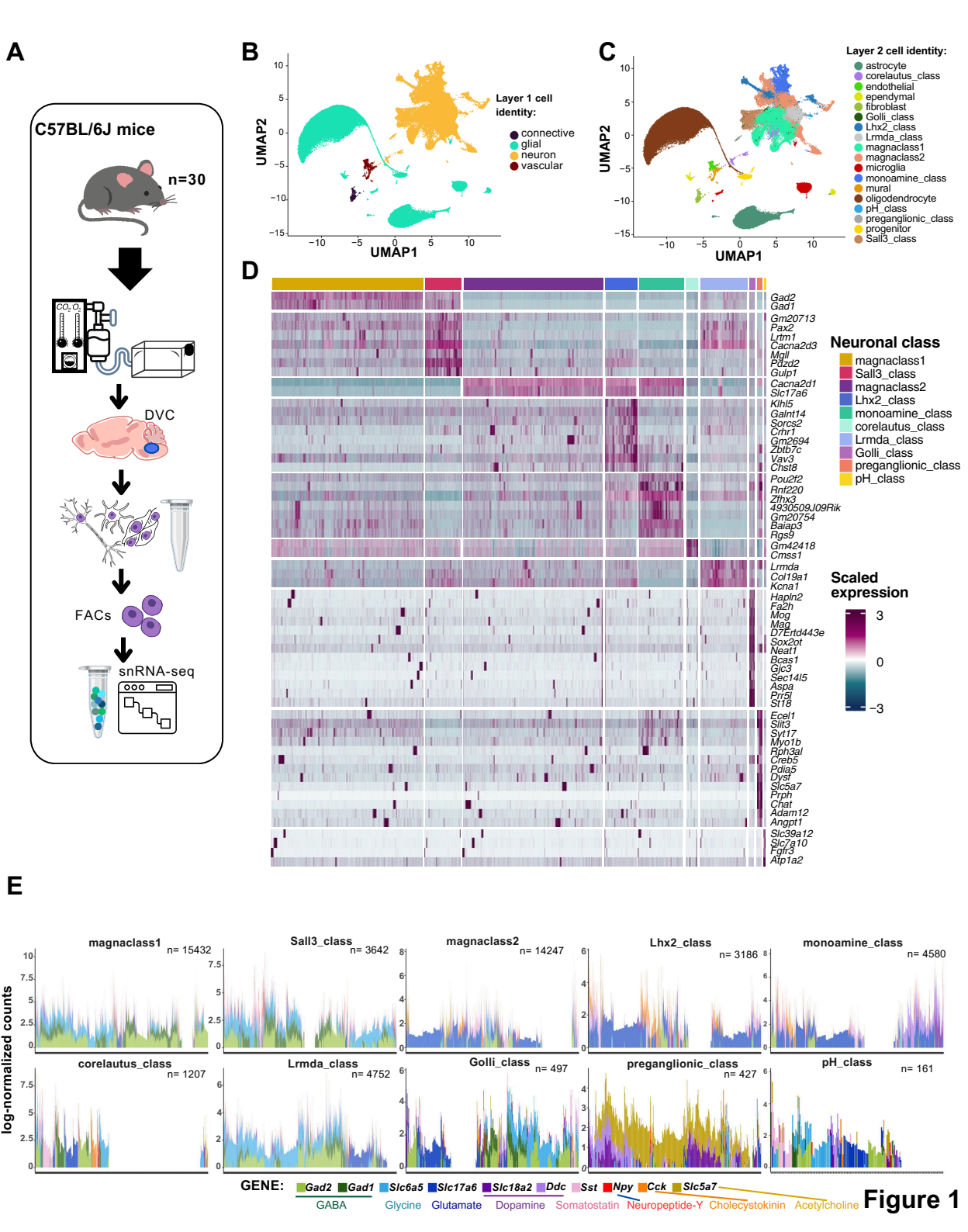
A
C57BL/6J mice
n=30
DVC
FACs
snRNA-seq
B
UMAP2
UMAP1
Layer 1 cell identity:
connective
glial
neuron
vascular
C
Layer 2 cell identity:
astrocyte
corelautus_class
endothelial
ependymal
fibroblast
Golli_class
Lhx2_class
Lrmda_class
magnaclass1
magnaclass2
microglia
monoamine_class
mural
oligodendrocyte
pH_class
preganglionic_class
progenitor
Sall3_class
D
Neuronal class
magnaclass1
Sall3_class
magnaclass2
Lhx2_class
monoamine_class
corelautus_class
Lrmda_class
Golli_class
preganglionic_class
pH_class
Scaled expression
Gad2
Gad1
Gm20713
Pax2
Lrtm1
Cacna2d3
Mgll
Pdzd2
Gulp1
Cacna2d1
Slc17a6
Klhl5
Galnt14
Sorcs2
Crhr1
Gm2694
Zbtb7c
Vav3
Chst8
Pou2f2
Rnf220
Zfhx3
4930509J09Rik
Gm20754
Baiap3
Rgs9
Gm42418
Cmss1
Lrmda
Col19a1
Kcna1
Hapln2
Fa2h
Mog
Mag
D7Ertd443e
Sox2ot
Neat1
Bcas1
Gjc3
Sec14l5
Aspa
Prrg1
St18
Ecel1
Slit3
Syt17
Myo1b
Rph3al
Creb5
Pdia5
Dyst
Slc5a7
Prph
Chat
Adam12
Angpt1
Slc39a12
Slc7a10
Fgfr3
Atp1a2
E
log-normalized counts
magnaclass1 n= 15432
Sall3_class n= 3642
magnaclass2 n= 14247
Lhx2_class n= 3186
monoamine_class n= 4580
corelautus_class n= 1207
Lrmda_class n= 4752
Golli_class n= 497
preganglionic_class n= 427
pH_class n= 161
GENE:
Gad2 Gad1 Slc6a5 Slc17a6 Slc18a2 Ddc Sst Npy Cck Slc5a7
GABA Glycine Glutamate Dopamine Somatostatin Neuropeptide-Y Cholecystokinin Acetylcholine

Figure 1

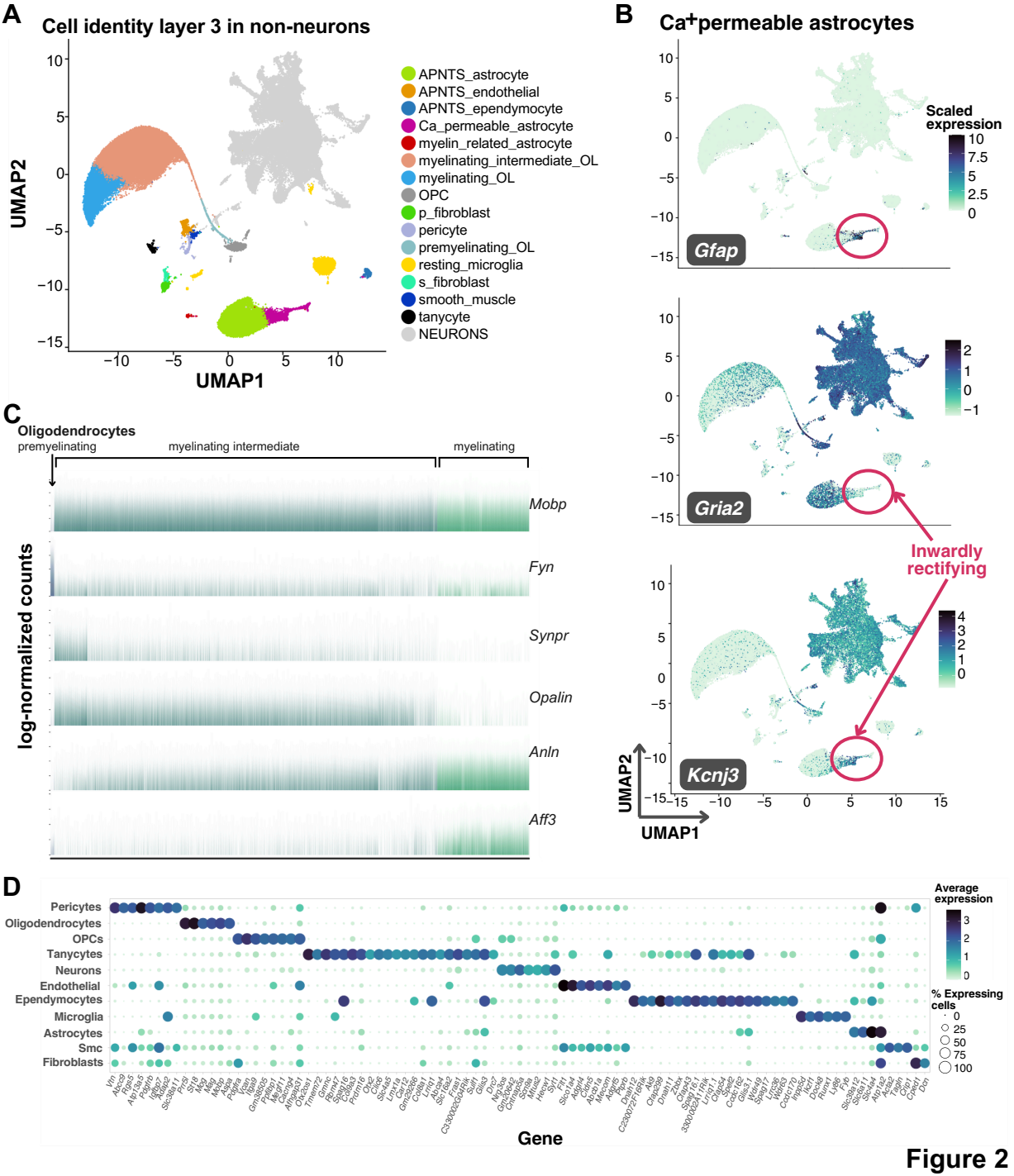
A
Cell identity layer 3 in non-neurons
UMAP2
UMAP1
APNTS_astrocyte
APNTS_endothelial
APNTS_ependymocyte
Ca_permeable_astrocyte
myelin_related_astrocyte
myelinating_intermediate_OL
myelinating_OL
OPC
p_fibroblast
pericyte
premyelinating_OL
resting_microglia
s_fibroblast
smooth_muscle
tanycyte
NEURONS
B
Ca+permeable astrocytes
Scaled expression
Gfap
Gria2
Kcnj3
Inwardly rectifying
UMAP2
UMAP1
C
Oligodendrocytes
premyelinating
myelinating intermediate
myelinating
log-normalized counts
Mobp
Fyn
Synpr
Opalin
Anln
Aff3
D
Pericytes
Oligodendrocytes
OPCs
Tanycytes
Neurons
Endothelial
Ependymocytes
Microglia
Astrocytes
Smc
Fibroblasts
Average expression
% Expressing cells
Gene

Figure 2

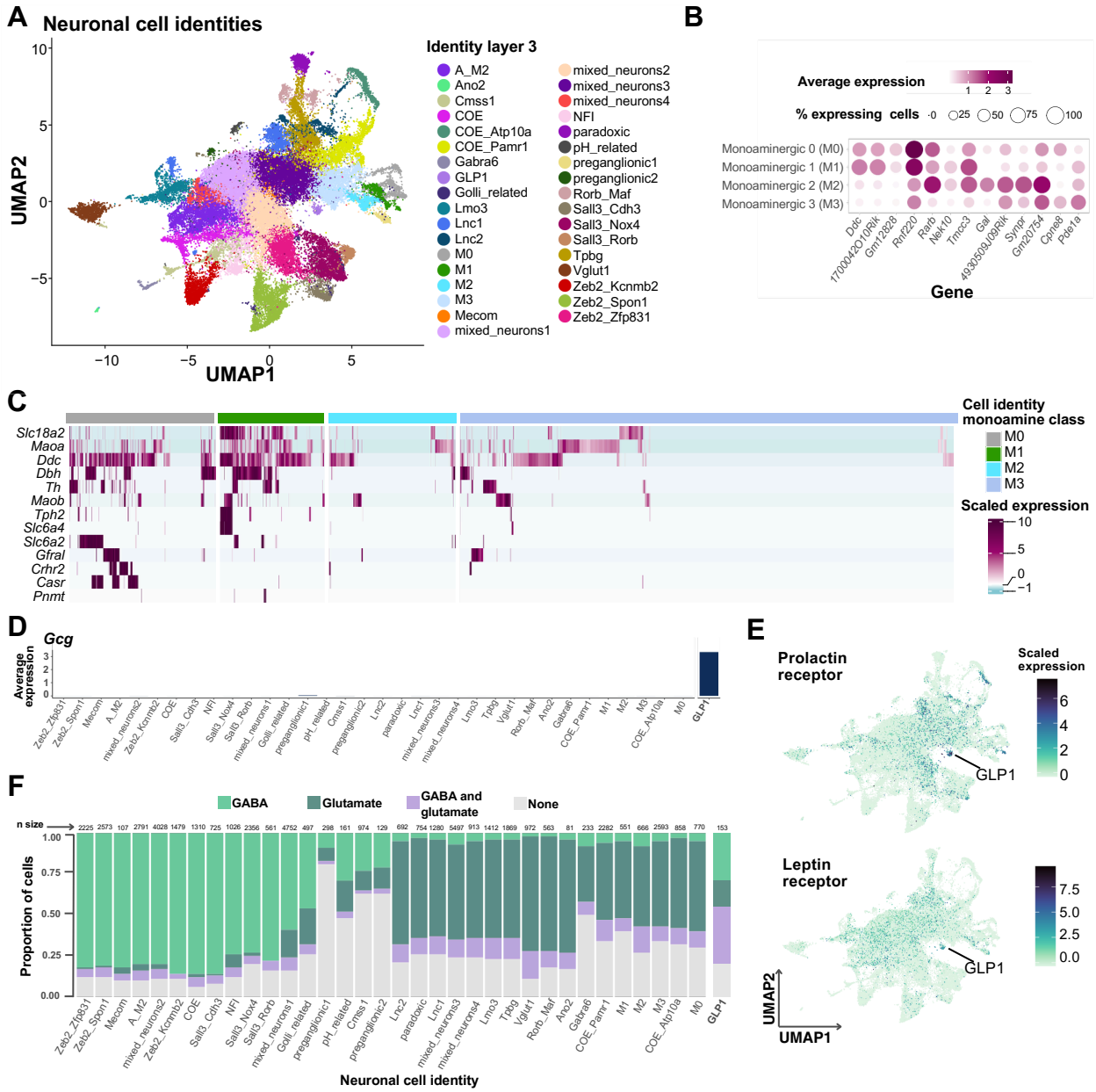
A
Neuronal cell identities
UMAP2
UMAP1
Identity layer 3
A_M2
Ano2
Cmss1
COE
COE_Atp10a
COE_Pamr1
Gabra6
GLP1
Golli_related
Lmo3
Lnc1
Lnc2
M0
M1
M2
M3
Mecom
mixed_neurons1
mixed_neurons2
mixed_neurons3
mixed_neurons4
NFI
paradoxic
pH_related
preganglionic1
preganglionic2
Rorb_Maf
Sall3_Cdh3
Sall3_Nox4
Sall3_Rorb
Tpbg
Vglut1
Zeb2_Kcnmb2
Zeb2_Spon1
Zeb2_Zfp831
B
Average expression
% expressing cells
Monoaminergic 0 (M0)
Monoaminergic 1 (M1)
Monoaminergic 2 (M2)
Monoaminergic 3 (M3)
Ddc
1700042O10Rik
Gm12828
Rnf220
Rarb
Nek10
Tmcc3
Gal
4930503J09Rik
Syngr
Gm20754
Cpne8
Pde1a
Gene
C
Slc18a2
Maoa
Ddc
Dbh
Th
Maob
Tph2
Slc6a4
Slc6a2
Gfral
Crhr2
Casr
Pnmt
Cell identity monoamine class
M0
M1
M2
M3
Scaled expression
D
Gcg
Average expression
E
Prolactin receptor
Leptin receptor
Scaled expression
GLP1
UMAP2
UMAP1
F
GABA
Glutamate
GABA and glutamate
None
n size
Proportion of cells
Neuronal cell identity

Figure 3

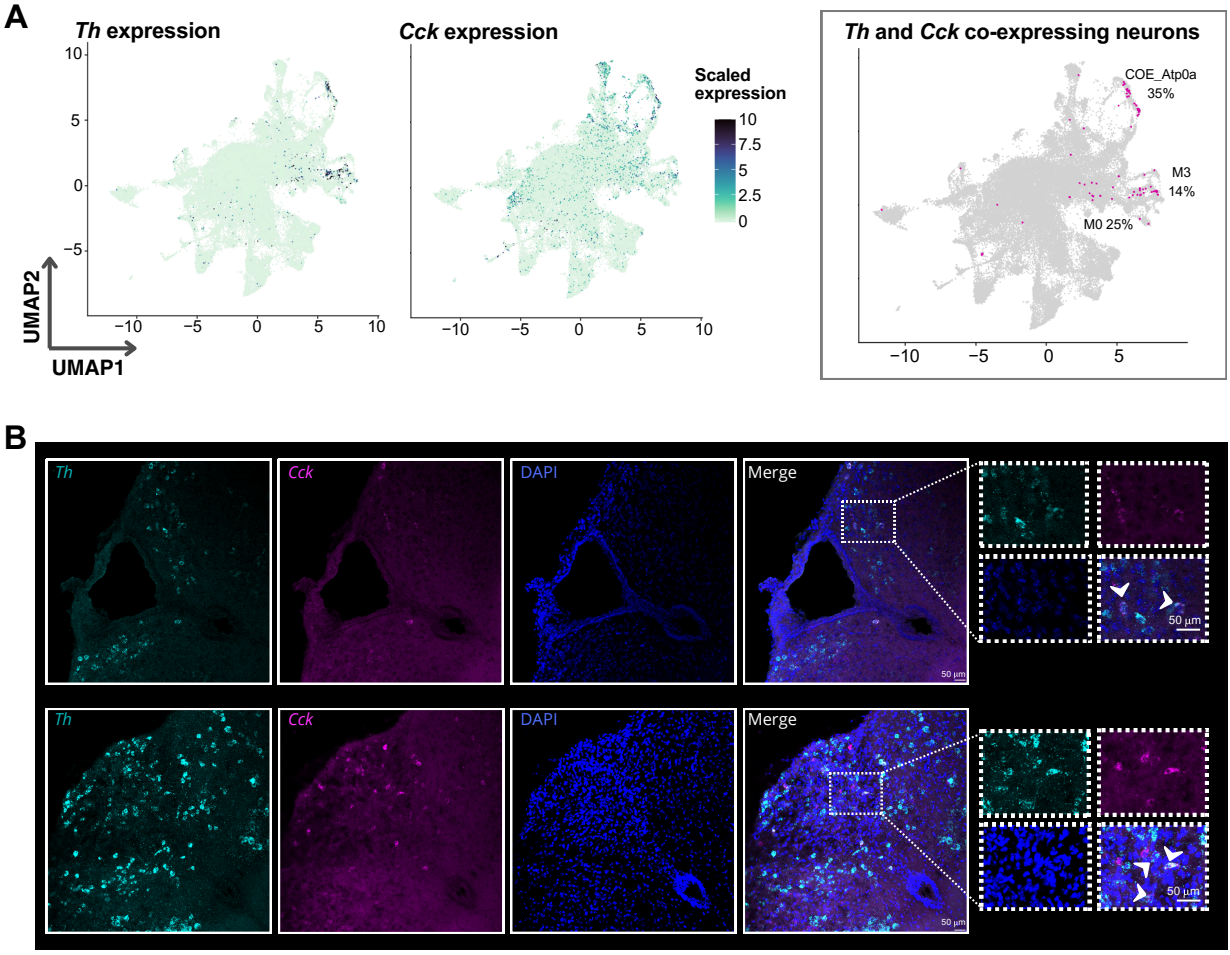
A
Th expression
Cck expression
Scaled expression
10
7.5
5
2.5
0
UMAP2
UMAP1
Th and Cck co-expressing neurons
COE_Atp0a
35%
M3
14%
M0 25%
B
Th
Cck
DAPI
Merge
50 µm

Figure 4

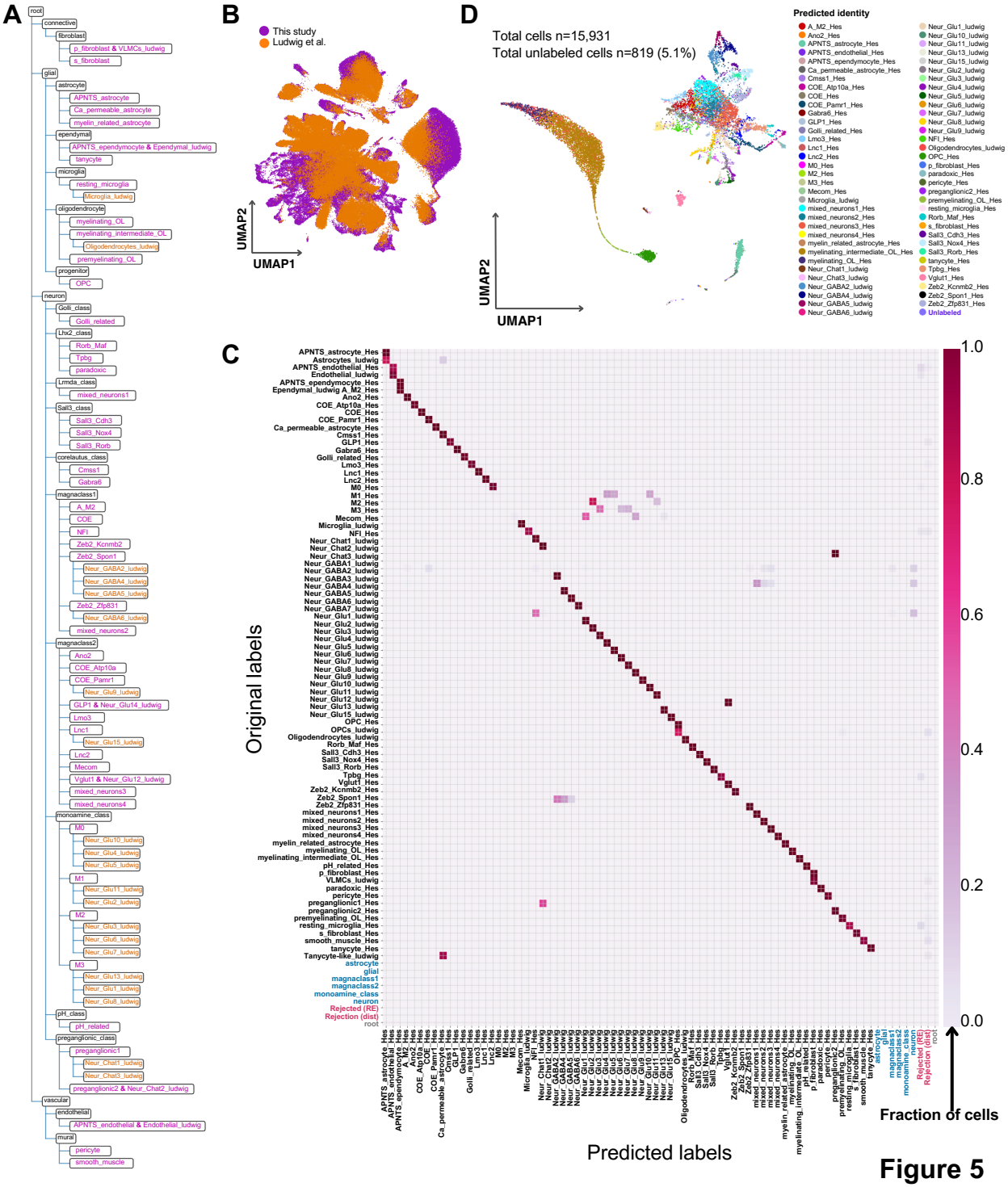
A
root
connective
fibroblast
p_fibroblast & VLMCs_ludwig
s_fibroblast
glial
astrocyte
APNTS_astrocyte
Ca_permeable_astrocyte
myelin_related_astrocyte
ependymal
APNTS_ependymocyte & Ependymal_ludwig
tanycyte
microglia
resting_microglia
Microglia_ludwig
oligodendrocyte
myelinating_OL
myelinating_intermediate_OL
Oligodendrocytes_ludwig
premyelinating_OL
progenitor
OPC
neuron
Golli_class
Golli_related
Lhx2_class
Rorb_Maf
Tpbg
paradoxic
Lrmda_class
mixed_neurons1
Sall3_class
Sall3_Cdh3
Sall3_Nox4
Sall3_Rorb
corelautus_class
Cmss1
Gabra6
magnaclass1
A_M2
COE
NFI
Zeb2_Kcnmb2
Zeb2_Spon1
Neur_GABA2_ludwig
Neur_GABA4_ludwig
Neur_GABA5_ludwig
Zeb2_Zfp831
Neur_GABA6_ludwig
mixed_neurons2
magnaclass2
Ano2
COE_Atp10a
COE_Pamr1
Neur_Glu9_ludwig
GLP1 & Neur_Glu14_ludwig
Lmo3
Lnc1
Neur_Glu15_ludwig
Lnc2
Mecom
Vglut1 & Neur_Glu12_ludwig
mixed_neurons3
mixed_neurons4
monoamine_class
M0
Neur_Glu10_ludwig
Neur_Glu4_ludwig
Neur_Glu5_ludwig
M1
Neur_Glu11_ludwig
Neur_Glu2_ludwig
M2
Neur_Glu3_ludwig
Neur_Glu6_ludwig
Neur_Glu7_ludwig
M3
Neur_Glu13_ludwig
Neur_Glu1_ludwig
Neur_Glu8_ludwig
pH_class
pH_related
preganglionic_class
preganglionic1
Neur_Chat1_ludwig
Neur_Chat3_ludwig
preganglionic2 & Neur_Chat2_ludwig
vascular
endothelial
APNTS_endothelial & Endothelial_ludwig
mural
pericyte
smooth_muscle
B
This study
Ludwig et al.
UMAP2
UMAP1
D
Total cells n=15,931
Total unlabeled cells n=819 (5.1%)
UMAP2
UMAP1
Predicted identity
A_M2_Hes
Ano2_Hes
APNTS_astrocyte_Hes
APNTS_endothelial_Hes
APNTS_ependymocyte_Hes
Ca_permeable_astrocyte_Hes
Cmss1_Hes
COE_Atp10a_Hes
COE_Hes
COE_Pamr1_Hes
Gabra6_Hes
GLP1_Hes
Golli_related_Hes
Lmo3_Hes
Lnc1_Hes
Lnc2_Hes
M0_Hes
M1_Hes
M2_Hes
M3_Hes
Mecom_Hes
Microglia_ludwig
mixed_neurons1_Hes
mixed_neurons2_Hes
mixed_neurons3_Hes
mixed_neurons4_Hes
myelin_related_astrocyte_Hes
myelinating_intermediate_OL_Hes
myelinating_OL_Hes
Neur_Chat1_ludwig
Neur_Chat3_ludwig
Neur_GABA2_ludwig
Neur_GABA4_ludwig
Neur_GABA5_ludwig
Neur_GABA6_ludwig
Neur_Glu1_ludwig
Neur_Glu2_ludwig
Neur_Glu3_ludwig
Neur_Glu4_ludwig
Neur_Glu5_ludwig
Neur_Glu6_ludwig
Neur_Glu7_ludwig
Neur_Glu8_ludwig
Neur_Glu9_ludwig
NFI_Hes
Oligodendrocytes_ludwig
OPC_Hes
p_fibroblast_Hes
paradoxic_Hes
pericyte_Hes
preganglionic2_Hes
premyelinating_OL_Hes
resting_microglia_Hes
Rorb_Maf_Hes
s_fibroblast_Hes
Sall3_Cdh3_Hes
Sall3_Nox4_Hes
Sall3_Rorb_Hes
tanycyte_Hes
Tpbg_Hes
Vglut1_Hes
Zeb2_Kcnmb2_Hes
Zeb2_Spon1_Hes
Zeb2_Zfp831_Hes
Unlabeled
C
Original labels
Predicted labels
Fraction of cells
1.0
0.8
0.6
0.4
0.2
0.0

Figure 5

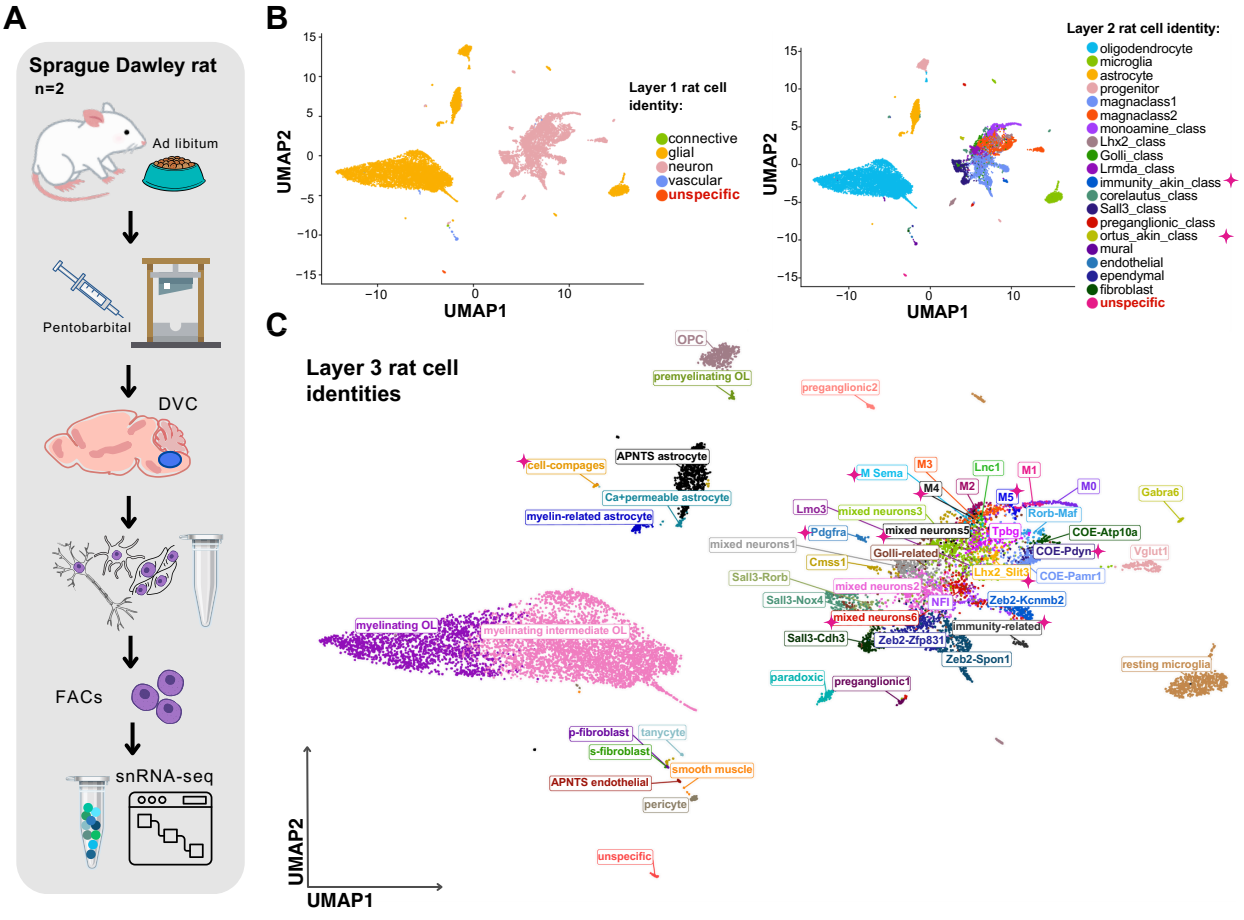
A
Sprague Dawley rat
n=2
Ad libitum
Pentobarbital
DVC
FACs
snRNA-seq
B
UMAP2
UMAP1
Layer 1 rat cell identity:
connective
glial
neuron
vascular
unspecific
Layer 2 rat cell identity:
oligodendrocyte
microglia
astrocyte
progenitor
magnaclass1
magnaclass2
monoamine_class
Lhx2_class
Golli_class
Lrmda_class
immunity_akin_class
corelautus_class
Sall3_class
preganglionic_class
ortus_akin_class
mural
endothelial
ependymal
fibroblast
unspecific
C
Layer 3 rat cell identities
OPC
premyelinating OL
preganglionic2
cell-compages
APNTS astrocyte
Ca+permeable astrocyte
myelin-related astrocyte
M Sema
M3
Lnc1
M1
M4
M2
M5
M0
Gabra6
Lmo3
mixed neurons3
Rorb-Maf
Pdgfra
mixed neurons5
Tpbg
COE-Atp10a
mixed neurons1
Golli-related
COE-Pdyn
Vglut1
Cmss1
Lhx2_Slit3
COE-Pamr1
Sall3-Rorb
mixed neurons2
Sall3-Nox4
NFI
Zeb2-Kcnmb2
mixed neurons6
immunity-related
Sall3-Cdh3
Zeb2-Zfp831
Zeb2-Spon1
resting microglia
paradoxic
preganglionic1
myelinating OL
myelinating intermediate OL
p-fibroblast
tanycyte
s-fibroblast
smooth muscle
APNTS endothelial
pericyte
unspecific
UMAP2
UMAP1

Figure 6

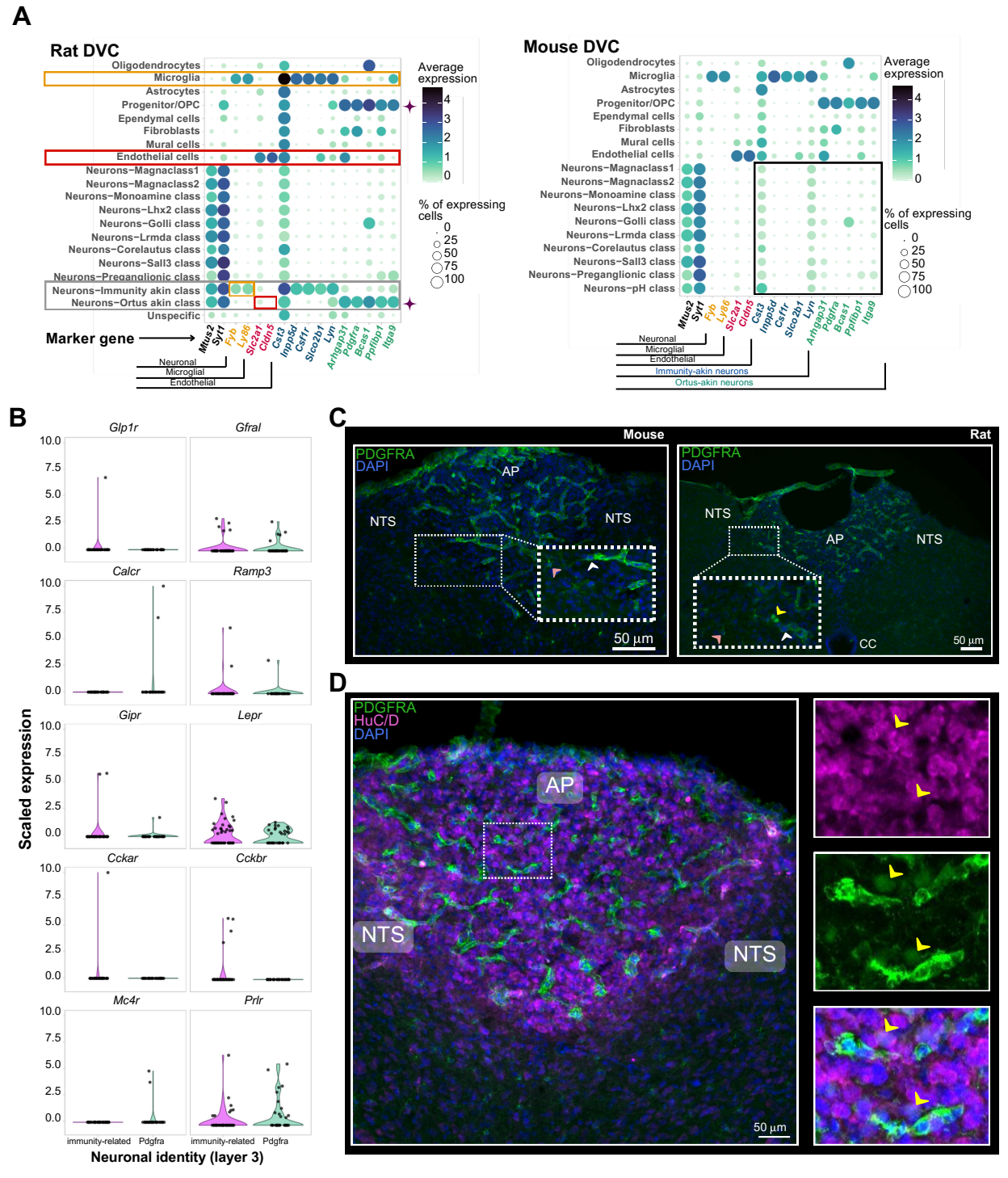
A
Rat DVC
Mouse DVC
Oligodendrocytes
Microglia
Astrocytes
Progenitor/OPC
Ependymal cells
Fibroblasts
Mural cells
Endothelial cells
Neurons−Magnaclass1
Neurons−Magnaclass2
Neurons−Monoamine class
Neurons−Lhx2 class
Neurons−Golli class
Neurons−Lrmda class
Neurons−Corelautus class
Neurons−Sall3 class
Neurons−Preganglionic class
Neurons−Immunity akin class
Neurons−Ortus akin class
Neurons−pH class
Unspecific
Average expression
% of expressing cells
Marker gene
Mtus2
Syt1
Fyb
Lyl6
Slc2a1
Cldn5
Cst3
Inpp5d
Csf1r
Slco2b1
Lyn
Arhgap31
Pdgfra
Bcas1
Ppfibp1
Itga9
Neuronal
Microglial
Endothelial
Immunity-akin neurons
Ortus-akin neurons
B
Glp1r
Gfral
Calcr
Ramp3
Gipr
Lepr
Cckar
Cckbr
Mc4r
Prlr
Scaled expression
immunity-related
Pdgfra
Neuronal identity (layer 3)
C
Mouse
Rat
PDGFRA
DAPI
AP
NTS
CC
50 µm
D
HuC/D

Figure 7

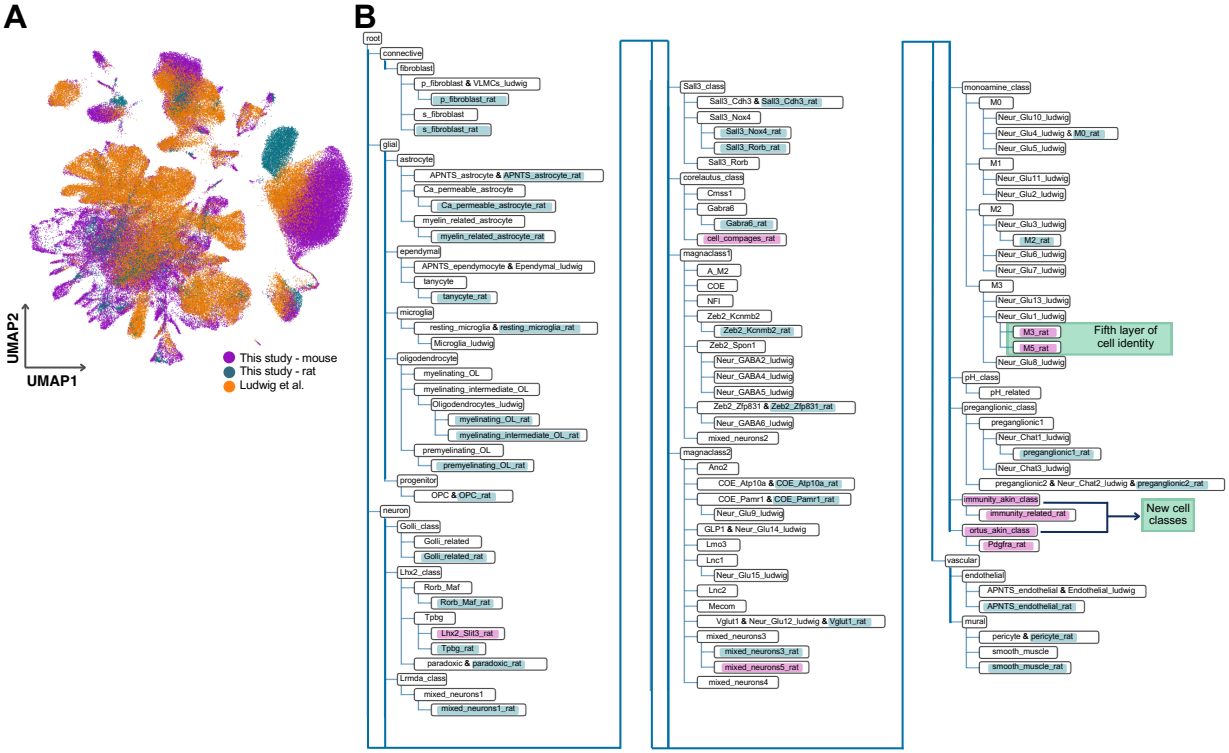
A
UMAP2
UMAP1
This study - mouse
This study - rat
Ludwig et al.
B
root
connective
fibroblast
p_fibroblast & VLMCs_ludwig
p_fibroblast_rat
s_fibroblast
s_fibroblast_rat
glial
astrocyte
APNTS_astrocyte & APNTS_astrocyte_rat
Ca_permeable_astrocyte
Ca_permeable_astrocyte_rat
myelin_related_astrocyte
myelin_related_astrocyte_rat
ependymal
APNTS_ependymocyte & Ependymal_ludwig
tanycyte
tanycyte_rat
microglia
resting_microglia & resting_microglia_rat
Microglia_ludwig
oligodendrocyte
myelinating_OL
myelinating_intermediate_OL
Oligodendrocytes_ludwig
myelinating_OL_rat
myelinating_intermediate_OL_rat
premyelinating_OL
premyelinating_OL_rat
progenitor
OPC & OPC_rat
neuron
Golli_class
Golli_related
Golli_related_rat
Lhx2_class
Rorb_Maf
Rorb_Maf_rat
Tpbg
Lhx2_Sitl3_rat
Tpbg_rat
paradoxic & paradoxic_rat
Lrmda_class
mixed_neurons1
mixed_neurons1_rat
Sall3_class
Sall3_Cdh3 & Sall3_Cdh3_rat
Sall3_Nox4
Sall3_Nox4_rat
Sall3_Rorb_rat
Sall3_Rorb
corelautus_class
Cmss1
Gabra6
Gabra6_rat
cell_compages_rat
magnaclass1
A_M2
COE
NF1
Zeb2_Kcnmb2
Zeb2_Kcnmb2_rat
Zeb2_Spon1
Neur_GABA2_ludwig
Neur_GABA4_ludwig
Neur_GABA5_ludwig
Zeb2_Zfp831 & Zeb2_Zfp831_rat
Neur_GABA6_ludwig
mixed_neurons2
magnaclass2
Anc2
COE_Atp10a & COE_Atp10a_rat
COE_Pamr1 & COE_Pamr1_rat
Neur_Glu9_ludwig
GLP1 & Neur_Glu14_ludwig
Lmo3
Lnc1
Neur_Glu15_ludwig
Lnc2
Mecom
Vglut1 & Neur_Glu12_ludwig & Vglut1_rat
mixed_neurons3
mixed_neurons3_rat
mixed_neurons5_rat
mixed_neurons4
monoamine_class
M0
Neur_Glu10_ludwig
Neur_Glu4_ludwig & M0_rat
Neur_Glu5_ludwig
M1
Neur_Glu11_ludwig
Neur_Glu2_ludwig
M2
Neur_Glu3_ludwig
M2_rat
Neur_Glu6_ludwig
Neur_Glu7_ludwig
M3
Neur_Glu13_ludwig
Neur_Glu1_ludwig
M3_rat
M5_rat
Fifth layer of cell identity
Neur_Glu8_ludwig
pH_class
pH_related
preganglionic_class
preganglionic1
Neur_Chat1_ludwig
preganglionic1_rat
Neur_Chat3_ludwig
preganglionic2 & Neur_Chat2_ludwig & preganglionic2_rat
immunity_akin_class
immunity_related_rat
ortus_akin_class
Pdgfra_rat
New cell classes
vascular
endothelial
APNTS_endothelial & Endothelial_ludwig
APNTS_endothelial_rat
mural
pericyte & pericyte_rat
smooth_muscle
smooth_muscle_rat

Figure 8

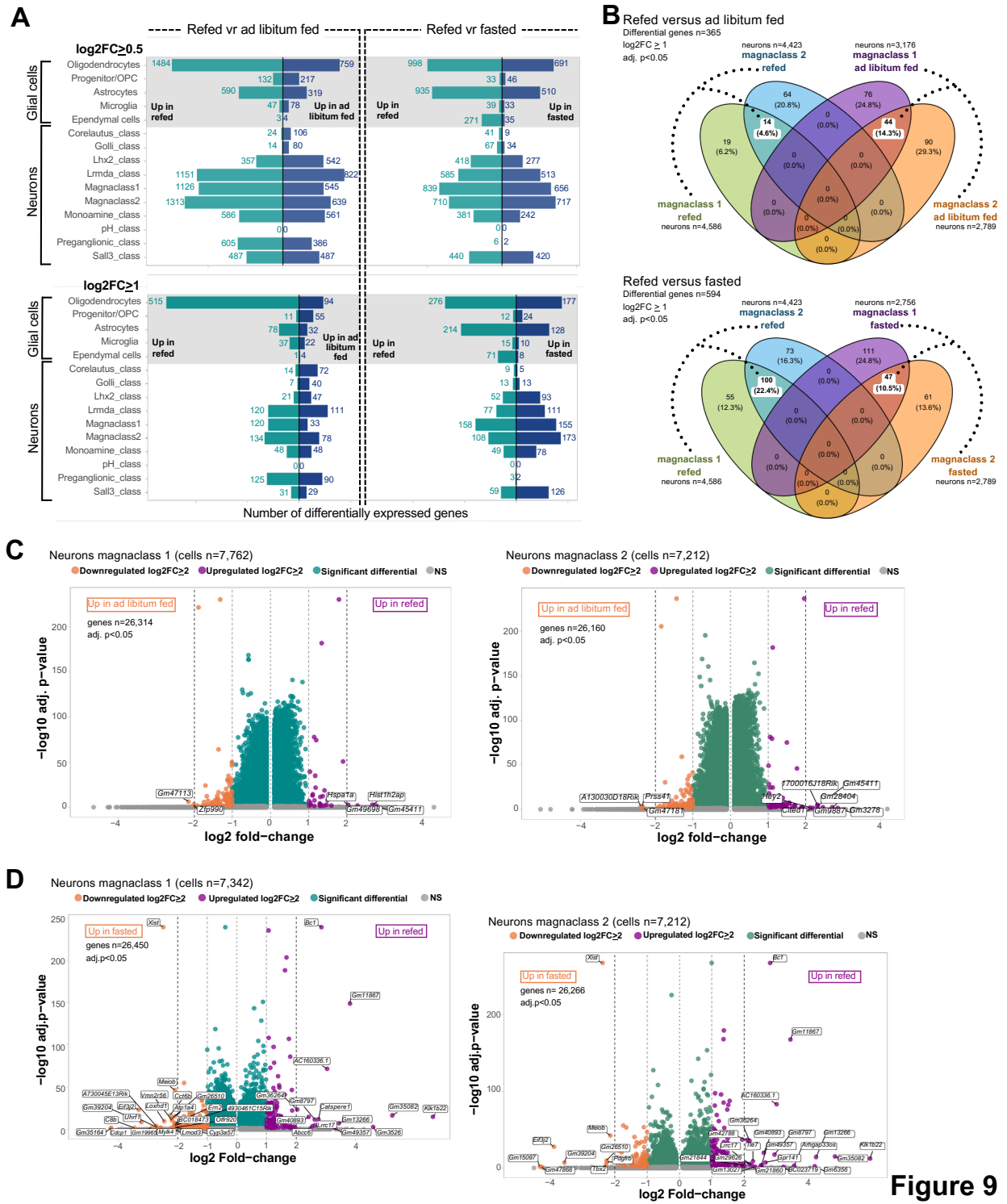
A
Refed vr ad libitum fed
Refed vr fasted
log2FC≥0.5
Glial cells
Neurons
Oligodendrocytes
Progenitor/OPC
Astrocytes
Microglia
Ependymal cells
Corelautus_class
Golli_class
Lhx2_class
Lrmda_class
Magnaclass1
Magnaclass2
Monoamine_class
pH_class
Preganglionic_class
Sall3_class
Up in refed
Up in ad libitum fed
Up in refed
Up in fasted
log2FC≥1
Up in refed
Up in ad libitum fed
Up in refed
Up in fasted
Number of differentially expressed genes
B
Refed versus ad libitum fed
Differential genes n=365
log2FC ≥ 1
adj. p<0.05
neurons n=4,423
magnaclass 2
refed
neurons n=3,176
magnaclass 1
ad libitum fed
magnaclass 1
refed
neurons n=4,586
magnaclass 2
ad libitum fed
neurons n=2,789
Refed versus fasted
Differential genes n=594
log2FC ≥ 1
adj. p<0.05
neurons n=4,423
magnaclass 2
refed
neurons n=2,756
magnaclass 1
fasted
magnaclass 1
refed
neurons n=4,586
magnaclass 2
fasted
neurons n=2,789
C
Neurons magnaclass 1 (cells n=7,762)
Downregulated log2FC≥2
Upregulated log2FC≥2
Significant differential
NS
Up in ad libitum fed
genes n=26,314
adj. p<0.05
Up in refed
−log10 adj. p−value
log2 fold−change
Neurons magnaclass 2 (cells n=7,212)
Up in ad libitum fed
genes n=26,160
adj. p<0.05
Up in refed
D
Neurons magnaclass 1 (cells n=7,342)
Up in fasted
genes n=26,450
adj.p<0.05
Up in refed
−log10 adj.p−value
log2 Fold−change
Neurons magnaclass 2 (cells n=7,212)
Up in fasted
genes n= 26,266
adj.p<0.05
Up in refed
−log10 adj.p−value
log2 Fold−change

Figure 9